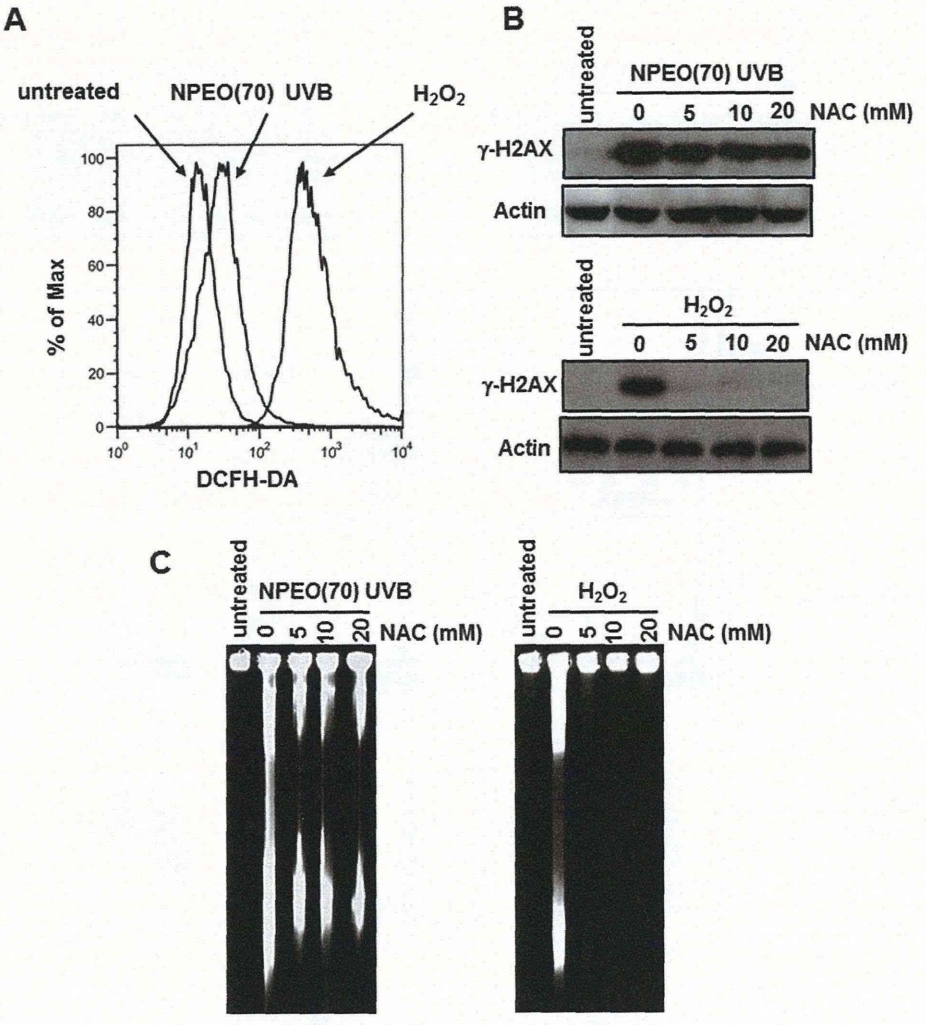

Fig. 4. Involvement of ROS in the generation of γ-H2AX by UVB-irradiated NPEO(70). (a) Cells incubated in the presence of 10 μM of DCFH-DA for 0.5 h were treated with UVB (500 J/cm^2)-irradiated NPEO(70) (300 μM) or H_2O_2 (3 mM) for 4 h. The fluorescence intensity of DCFH-DA was analysed by FCM. (b) Cells incubated with NAC (5–20 mM) for 30 min were treated with UVB-irradiated (500 J/cm^2) NPEO(70) (300 μM) or H_2O_2 (3 mM) for 4 h. Actin is a standard for equal loading. (c) Cells were treated as same as (b), and BSFGE was carried out.

Discussion

γ-H2AX is currently attracting attention as a new biomarker for detecting genotoxic insults (27,28). Based on γ-H2AX, we recently showed the genotoxic effect of NPEOs where the ability to form γ-H2AX was strongly dependent on the number of EO units (21). In this study, we have for the first time clarified that UVB irradiation drastically changed the genotoxic potential of NPEO(15) and NPEO(70). NPEO(15) showed great ability to generate γ-H2AX, which was reduced by UVB irradiation (Figure 2e). On the other hand, non-genotoxic NPEO(70) became able to generate γ-H2AX after UVB irradiation (Figure 2c). Since the ability to generate γ-H2AX depends largely on the number of EO units (21), the production of γ-H2AX by UVB-irradiated NPEO(70) would be a result of the NPEOs having fewer EO units. Indeed, HPLC analysis of UVB-irradiated NPEO(70) suggested the presence of around 15 EO units (Figure 5a). Actually, our previous study clarified that an NPEO with 15 EO units had the greatest ability to generate γ-H2AX (21). Gradual elevated levels of γ-H2AX in UVB-irradiated NPEO(70) would be due to gradual generation of NPEOs having EO units around 15.

In the case of NPEO(15) and NPEO(70) irradiated with over 500 J/cm^2 of UVB, there are two possible explanations for the attenuated generation of γ-H2AX. One reason would be destruction of the benzene ring. The HPLC peak detected by absorbance of 275 nm (benzene exhibits a sharp absorption waveform in the neighbourhood of 275 nm) gradually decreased after UVB irradiation (Figure 5), which was well consistent with the result of decreased generation of γ-H2AX. Another reason is the change in solubility resulting from fewer hydrophilic EO units. NPEOs with a smaller number of EO units ($n < 15$) become less soluble in culture medium resulting in the formation of particulate aggregates, which might cause a decrease in the cellular uptake of NPEOs. Around 15 EO units might be a suitable number for good solubility in culture medium and for cellular uptake.

Although our previous study suggested that generation of ROS by UVB irradiation was involved in the photodegradation of NPEO(70) (9), the exact reason why photodegradation of NPEO(70) started from the EO units near the benzene ring

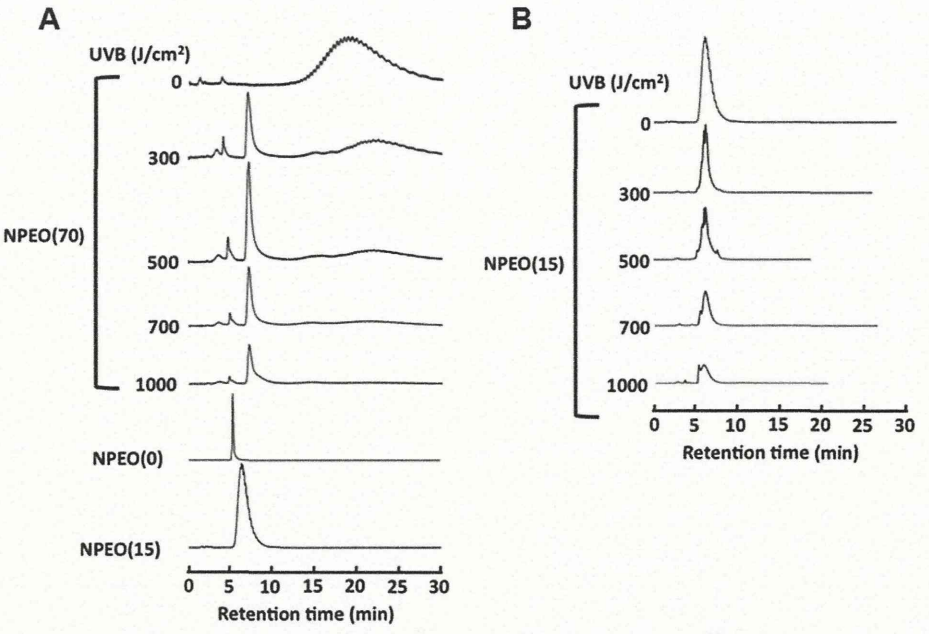

Fig. 5. HPLC analysis of UVB-irradiated NPEOs. UVB (100–1000 J/cm²)-irradiated (a) NPEO(15) and (b) NPEO(70) were analysed using HPLC.

was not clarified. In addition, the formation of intermediates other than shortened NPEOs has yet to be examined. Chen *et al.* (7) suggested that, in addition to the shortening of the EO side chains and benzene ring's destruction in NPEO(10), UV irradiation led to the generation of intermediates having carboxylatedethoxylate and hydrogenation of the benzene ring, and cyclohexane compounds. Furthermore, Castillo *et al.* (8) revealed the generation of phenolethoxycarboxylate, methoxyphenolethoxycarboxylate and ethoxyphenylheptanoic acid as intermediates after UV irradiation in NPEO(9). Further study will be needed to elucidate whether any photooxidised or degraded intermediates derived from NPEO(70) were produced and involved in the generation of γ-H2AX.

An inhibitor study using caffeine and wortmannin showed that histone H2AX was phosphorylated via ATM or DNA-PK activation, a general signalling pathway in response to DSBs, after treatment with UVB-irradiated NPEO(70) (Figure 3d). However, the mechanism by which the UVB-irradiated NPEO(70) generated γ-H2AX, or in other words, how UVB-irradiated NPEO(70) forms DSBs is unclear but worth studying. The generation of γ-H2AX by UVB-irradiated NPEO(70) was slightly attenuated in the presence of NAC, suggesting ROS to be partially involved. ROS generates oxidative bases and SSBs, which can be converted into DSBs as a consequence of the collision of the replication forks (13,14). Therefore, if oxidative bases formed, γ-H2AX would be detected in S phase (if oxidative bases were the major DNA damage generated by UVB-irradiated NPEO(70), γ-H2AX would be mainly detected in S phase). However, γ-H2AX was detected throughout the cell cycle (Figure 3c). This suggested that ROS are not the main cause of γ-H2AX. Although γ-H2AX is also produced by DNA fragmentation during apoptosis (29), caspase-3 activation was not observed after treatment with UVB-irradiated NPEO(70) in the time frame examined (0.5–4 h) (data not shown). Thus, the generation of γ-H2AX might be independent of apoptotic DNA fragmentation. In addition, as physical breaks of DNA by photodegraded NPEO(70) in cell-free DNA (plasmid relaxation assay) were not observed (data not shown), the generation of γ-H2AX was considered attributable to undefined reasons which require cellular events. Recent review article by Costes *et al.* (30) suggested that generation of γ-H2AX is modulated by chromatin structures.γ-H2AX foci were more likely to be generated in euchromatin than in heterochromatin after ionising radiation (31,32). In this study, γ-H2AX foci generated by UVB-irradiated NPEO(70) were mainly located in non-dense DNA regions (Figure 2a). They also suggested that γ-H2AX foci do not always represent mark of DSBs, but damaged chromatin architecture and/or undergoing remodelling chromatin (30). Further study will be needed to elucidate the mechanisms involved.

In summary, we clarified that UVB irradiation altered the capacity of NPEOs to generate γ-H2AX. The production of γ-H2AX means the formation of DSBs, the worst type of DNA damage. The unscheduled generation of DSBs by extrinsic insult may result in an increased risk of misrepair. Notably, damage in a critical gene related to cancer (such as a tumour suppressor gene) could have catastrophic consequences for the cell. It would be no problem if toxic substances were degraded by sunlight and neutralised like NPEO(15). However, some non-toxic compounds become genotoxic in the process of photodegradation. In addition to NPEO(70), our previous studies suggested that several environmental chemicals become more genotoxic with photodegradation (6,17,18). One should pay attention to the possibility that exposure to sunlight can change chemicals into forms with the potential for genotoxicity.

Supplementary data

Supplementary Figures 1–3 are available at *Mutagenesis* Online.

Funding

This work was supported in part by Grants-in-aid for Young Scientific Research (B) (#22710065), for Scientific Research

(C) (#21510071) from the Ministry of Education, Culture, Sports, Science and Technology, and for Research on Risk of Chemical Substances from the Ministry of Health, Labor, and Welfare of Japan.

References

1. Soares, A., Guieysse, B., Jefferson, B., Cartmell, E. and Lester, J. N. (2008) Nonylphenol in the environment: a critical review on occurrence, fate, toxicity and treatment in wastewaters. *Environ. Int.,* **34**, 1033–1049.
2. Ying, G. G. (2006) Fate, behavior and effects of surfactants and their degradation products in the environment. *Environ. Int.,* **32**, 417–431.
3. Sharma, V. K., Anquandah, G. A., Yngard, R. A., Kim, H., Fekete, J., Bouzek, K., Ray, A. K. and Golovko, D. (2009) Nonylphenol, octylphenol, and bisphenol-A in the aquatic environment: a review on occurrence, fate, and treatment. *J. Environ. Sci. Health A Tox. Hazard Subst. Environ. Eng.,* **44**, 423–442.
4. Ying, G. G., Williams, B. and Kookana, R. (2002) Environmental fate of alkylphenols and alkylphenol ethoxylates – a review. *Environ. Int.,* **28**, 215–226.
5. Kim, J., Park, J., Kim, P. G., Lee, C., Choi, K. and Choi, K. (2010) Implication of global environmental changes on chemical toxicity-effect of water temperature, pH, and ultraviolet B irradiation on acute toxicity of several pharmaceuticals in *Daphnia magna*. *Ecotoxicology,* **19**, 662–669.
6. Ohnuki, G., Toyooka, T. and Ibuki, Y. (2010) UVB in solar-simulated light causes formation of BaP-photoproducts capable of generating phosphorylated histone H2AX. *Mutat. Res.,* **702**, 70–77.
7. Chen, L., Zhou, H. Y. and Deng, Q. Y. (2007) Photolysis of nonylphenol ethoxylates: the determination of the degradation kinetics and the intermediate products. *Chemosphere,* **68**, 354–359.
8. Castillo, M., Penuela, G. and Barcelo, D. (2001) Identification of photocatalytic degradation products of non-ionic polyethoxylated surfactants in wastewaters by solid-phase extraction followed by liquid chromatography-mass spectrometric detection. *Fresenius J. Anal. Chem.,* **369**, 620–628.
9. Goto, R., Kubota, T., Ibuki, Y., Kaji, K. and Goto, A. (2004) Degradation of nonylphenol polyethoxylates by ultraviolet B irradiation and effects of their products on mammalian cultured cells. *Toxicology,* **202**, 237–247.
10. Nimrod, A. C. and Benson, W. H. (1996) Environmental estrogenic effects of alkylphenol ethoxylates. *Crit. Rev. Toxicol.,* **26**, 335–364.
11. Balch, G. and Metcalfe, C. (2006) Developmental effects in Japanese medaka (*Oryzias latipes*) exposed to nonylphenol ethoxylates and their degradation products. *Chemosphere,* **62**, 1214–1223.
12. Rogakou, E. P., Pilch, D. R., Orr, A. H., Ivanova, V. S. and Bonner, W. M. (1998) DNA double-stranded breaks induce histone H2AX phosphorylation on serine 139. *J. Biol. Chem.,* **273**, 5858–5868.
13. Bonner, W. M., Redon, C. E., Dickey, J. S., Nakamura, A. J., Sedelnikova, O. A., Solier, S. and Pommier, Y. (2008) GammaH2AX and cancer. *Nat. Rev. Cancer,* **8**, 957–967.
14. Mah, L. J., El-Osta, A. and Karagiannis, T. C. (2010) gammaH2AX: a sensitive molecular marker of DNA damage and repair. *Leukemia,* **24**, 679–686.
15. Toyooka, T. and Ibuki, Y. (2009) Cigarette sidestream smoke induces phosphorylated histone H2AX. *Mutat. Res.,* **676**, 34–40.
16. Ishihama, M., Toyooka, T. and Ibuki, Y. (2008) Generation of phosphorylated histone H2AX by benzene metabolites. *Toxicol. In Vitro,* **22**, 1861–1868.
17. Ibuki, Y., Tani, Y. and Toyooka, T. (2008) UVB-exposed chlorinated bisphenol A generates phosphorylated histone H2AX in human skin cells. *Chem. Res. Toxicol.,* **21**, 1770–1776.
18. Toyooka, T., Ohnuki, G. and Ibuki, Y. (2008) Solar-simulated light-exposed benzo[*a*]pyrene induces phosphorylation of histone H2AX. *Mutat. Res.,* **650**, 132–139.
19. Toyooka, T. and Ibuki, Y. (2006) New method for testing phototoxicity of polycyclic aromatic hydrocarbons. *Environ. Sci. Technol.,* **40**, 3603–3608.
20. Toyooka, T., Ishihama, M. and Ibuki, Y. (2011) Phosphorylation of histone H2AX is a powerful tool for detecting chemical photogenotoxicity. *J. Invest. Dermatol.,* **131**, 1313–1321.
21. Toyooka, T., Kubota, T. and Ibuki, Y. (2012) Nonylphenol polyethoxylates induce phosphorylation of histone H2AX. *Mutat. Res.,* **741**, 57–64.
22. Soto A. M., Justicia, H., Wray, J. W. and Sonnenschein, C. (1991) p-Nonyl-phenol: an estrogenic xenobiotic released from "modified" polystyrene. *Environ. Health Perspect.*, **92**, 167–173.
23. Tanaka, T., Huang, X., Halicka, H. D., Zhao, H., Traganos, F., Albino, A. P., Dai, W. and Darzynkiewicz, Z. (2007) Cytometry of ATM activation and histone H2AX phosphorylation to estimate extent of DNA damage induced by exogenous agents. *Cytometry A.*, **71**, 648–661.
24. Kataoka, Y., Bindokas, V. P., Duggan, R. C., Murley, J. S. and Grdina, D. J. (2006) Flow cytometric analysis of phosphorylated histone H2AX following exposure to ionizing radiation in human microvascular endothelial cells. *J. Radiat. Res.,* **47**, 245–257.
25. Burma, S., Chen, B. P., Murphy, M., Kurimasa, A. and Chen, D. J. (2001) ATM phosphorylates histone H2AX in response to DNA double-strand breaks. *J. Biol. Chem.,* **276**, 42462–42467.
26. Okamoto, Y., Hayashi, T., Matsumami, S., Ueda, K., Toda, C., Kawanishi, S. and Kojima, N. (2006) Formation of DNA damaging product from light-irradiated nonylphenol. *J. Health Sci.,* **52**, 91–95.
27. Dickey, J. S., Redon, C. E., Nakamura, A. J., Baird, B. J., Sedelnikova, O. A. and Bonner, W. M. (2009) H2AX: functional roles and potential applications. *Chromosoma,* **118**, 683–692.
28. Kuo, L. J. and Yang, L. X. (2008) Gamma-H2AX – a novel biomarker for DNA double-strand breaks. *In Vivo*, **22**, 305–309.
29. Rogakou, E. P., Nieves-Neira, W., Boon, C., Pommier, Y. and Bonner, W. M. (2000) Initiation of DNA fragmentation during apoptosis induces phosphorylation of H2AX histone at serine 139. *J. Biol. Chem.,* **275**, 9390–9395.
30. Costes, S. V., Chiolo, I., Pluth, J. M., Barcellos-Hoff, M. H. and Jakob, B. (2010) Spatiotemporal characterization of ionizing radiation induced DNA damage foci and their relation to chromatin organization. *Mutat. Res.,* **704**, 78–87.
31. Costes, S. V., Ponomarev, A., Chen, J. L., Nguyen, D., Cucinotta, F. A., Barcellos-Hoff, M. H. (2007) Image-based modeling reveals dynamic redistribution of DNA damage into nuclear sub-domains. *PLoS Comput. Biol.,* **3**, e155.
32. Cowell, I. G., Sunter, N. J., Singh, P. B., Austin, C. A., Durkacz, B. W. and Tilby, M. J. (2007) gammaH2AX foci form preferentially in euchromatin after ionising-radiation. *PLoS One,* **2**, e1057.

Photochemistry and Photobiology, 2013, 89: 461–467

Nonylphenol Polyethoxylates Degraded by Three Different Wavelengths of UV and Their Genotoxic Change—Detected by Generation of γ-H2AX

Toru Kubota, Tatsushi Toyooka and Yuko Ibuki*

Institute for Environmental Sciences, University of Shizuoka, Shizuoka-shi, Shizuoka, Japan

Received 18 June 2012, accepted 19 September 2012, DOI: 10.1111/php.12002

ABSTRACT

UV rays in sunlight are an important factor in the degradation of chemicals. In this study, we investigated the degradation of nonionic surfactants, nonylphenol polyethoxylates (NPEOs) with 10 or 70 ethylene oxide (EO) units using UVA, B and C, and their genotoxic change based on phosphorylation of histone H2AX (γ-H2AX), a marker of DNA damage. NPEOs were degraded dependent on the energy of UV, that is, UVC having the highest energy was most effective, whereas UVA having the lowest energy caused little change. The EO side chain of NPEO (70) was broken near the benzene ring by UV, producing NPEOs with a shortened EO chain (around 10 units). The generation of γ-H2AX reflected the pattern of degradation; shortening of the EO chain changed NPEO(70) into an inducer for γ-H2AX, and degradation of NPEO(10) attenuated the genotoxicity. The γ-H2AX generated by NPEO(10) and UV-degraded NPEO(70) was independent of the cell cycle. The formation of DNA double strand breaks detected by gel electrophoresis was consistent with the results for γ-H2AX. These results suggested that UV rays can make NPEOs harmless or genotoxic according to the degradation of the EO side chain, the effects being dependent on wavelength.

INTRODUCTION

The use of synthetic detergents is increasing every year. Nonylphenol polyethoxylates (NPEO(n), where n is the number of ethylene oxide units [EO]) are widely used as nonionic surfactants in detergents for industrial and household use. Because of the large scale of their use, organic materials in waste water are contaminated by NPEOs (1–4). NPEOs released in environments are broken down by microorganisms; first, aerobically into nonylphenol di- and monoethoxylates, then, anaerobically into nonylphenols (4,5). The biodegraded products are stable, and have been reported to be toxic to both marine and freshwater species (5,6).

Natural sunlight can cause the transformation of NPEOs. Ultraviolet (UV) rays in sunlight have proven effective at degrading both NPEOs and biodegraded nonylphenols (7–9). The UV spectrum can be divided into three based on wavelength: UVA (320–400 nm), UVB (280–320 nm) and UVC (200–280 nm). UVC is absorbed by the ozone layer and does not reach the earth. The shorter wavelength UVB has higher energy than UVA, and consequently, contributes to the photodegradation of chemical compounds in the environment (10,11). On exposure to UVB, NPEOs showed characteristic degradation patterns dependent on the lengths of their EO chains (7). However, UV wavelength-dependent degradation and changes of toxicity have not been examined.

Our recent study found that UVB made nongenotoxic NPEOs genotoxic by shortening of EO units (12). NPEOs with short degraded EO chains produced by exposure to UVB, induced serious DNA damage, DNA double strand breaks (DSBs). We also have elucidated the genotoxic potential of NPEO(n) having various EO units (n = 0–70); the genotoxicity was strongly dependent on the number of EO units, that is, NPEOs having fewer EO units (n = 0–15) showed a strong ability to induce DNA damage, whereas NPEOs with longer side chains like NPEO(70) had attenuated genotoxicity (13). Promotion of carcinogenesis by nonylphenols was reported *via* a mechanism involving the stimulation of cell proliferation and induction of oxidative DNA damage (14,15). Therefore, DNA damage induced by NPEOs degraded by UV is an important target for further risk assessments.

We have been using the phosphorylation of histone H2AX (γ-H2AX) as a marker for DNA damage. The generation of γ-H2AX, originally identified as an early event after the direct formation of DSBs by ionizing radiation (16), is now considered to occur also after the indirect formation of DSBs caused by the collision of the replication forks at sites of DNA damage including oxidative bases, DNA adducts, etc. (17,18). We previously reported that γ-H2AX was generated following the exposure of cells to various suspected DNA-damaging agents including several environmental chemicals and pharmacological agents (19–24). In addition to the advantage that γ-H2AX can be detected in response to many types of DNA damage, we and other researchers are convinced that γ-H2AX provides a considerably more sensitive and convenient measurement of DNA damage than other techniques such as pulse field gel electrophoresis and comet assays (17,18).

In this study, we analyzed the degradation of NPEO(10) and (70) after exposure to different wavelengths of UV (UVA, B and C), and the correlation with their genotoxic change. The genotoxicity of degraded NPEOs was examined based on the generation of γ-H2AX.

MATERIALS AND METHODS

NPEOs and UV irradiation. NPEO(n) (n = 10 and 70) kindly provided by NOF Co., Japan, were dissolved in water at a concentration of 10 mM, and exposed to UV in a glass dish 15 mm in diameter and 10 mm in height (1 mL per dish). To avoid water evaporation, the glass dish was sealed with UV-transmittable film (Dura Seal™: Diversified Biotech, Dedham, MA). A UVA lamp (HP-30LM; Atto Co., Japan) with

*Corresponding author email: ibuki@u-shizuoka-ken.ac.jp (Yuko Ibuki)

an emission wavelength of 320–380 nm and maximum peak of 365 nm, a UVB lamp (HP-30LM; Atto) with a 280–320 nm emission and maximum peak of 312 nm and a UVC lamp (HP-30C; Atto) with a 180–280 nm emission and maximum peak of 254 nm were used without cutoff filter. The spectra were shown in our previous study (25). During the exposure, fluences were simultaneously measured and integrated using a radiometer (ATV-3W; Atto) with 365, 312 and 254 nm detectors placed at the same distance as the glass dish from the UV source. The approximate irradiances of UVA, UVB and UVC at the sample level were 4.6, 8.5 and 8.2 J cm^{-2} h^{-1}, respectively.

Analysis of NPEOs degraded by UV irradiation. The degraded NPEOs were detected using high performance liquid chromatography (HPLC). The conditions for the HPLC analysis were given in a previous study (7). In brief, NPEOs and UV-degraded products were separated on a silica column (TSKgel Silica-150 [4.6 mmID × 25 cm]). The mobile phase solvent A was 30% acetonitrile and solvent B was 80% acetonitrile. Elution was carried out with a liner gradient from 100% A to 100% B over 30 min.

Cells and culture conditions. The human breast adenocarcinoma cell line MCF-7 (provided by Japanese Collection of Research Bioresources, Japan) was maintained in Dulbecco's modified Eagle's medium (DMEM) supplemented with 10% fetal bovine serum and 100 U mL^{-1} of penicillin/streptomycin at 37°C in an atmosphere of 5% CO_2. All experiments were performed with exponentially growing cells.

Immunofluorescence staining for detection of γ-H2AX. The cells treated with UV-irradiated NPEOs in Lab-Tek chamber slides (Nalge Nunc, IL) were immediately fixed in 2% paraformaldehyde for 30 min at room temperature and then in 100% methanol for 20 min at −20°C. Fixed cells were immersed in buffer containing 100 mM Tris-HCl, 50 mM EDTA and 0.5% Triton X-100 for 5 min at room temperature for better permealization, and blocked with 1% bovine serum albumin (BSA) for 30 min at 37°C. Cells were incubated with a primary antibody against phospho-H2AX (mouse monoclonal) (Millipore Bedford, MA, 1:200) for 2 h, then with a secondary antibody conjugated with fluorescein isothiocyanate (FITC) (Jackson Immuno Research Laboratories, PA). To confirm the distribution of foci, the nucleus was stained with propidium iodide (PI) (20 μg mL^{-1}). Images were acquired on a fluorescence microscope (BX51, Olympus, Japan).

Western blot analysis of γ-H2AX. The cells treated with UV-irradiated NPEOs were lysed in lysis buffer (50 mM Tris [pH 8.0], 5 mM EDTA, 150 mM NaCl, 0.5% Nonidet P-40 and 1 mM phenylmethylsulfonyl fluoride [PMSF]). The samples were separated by 12.5% SDS-PAGE, and blotted onto polyvinylidine fluoride (PVDF) membranes. After blocking with 1% nonfat milk, the membranes were incubated overnight at 4°C

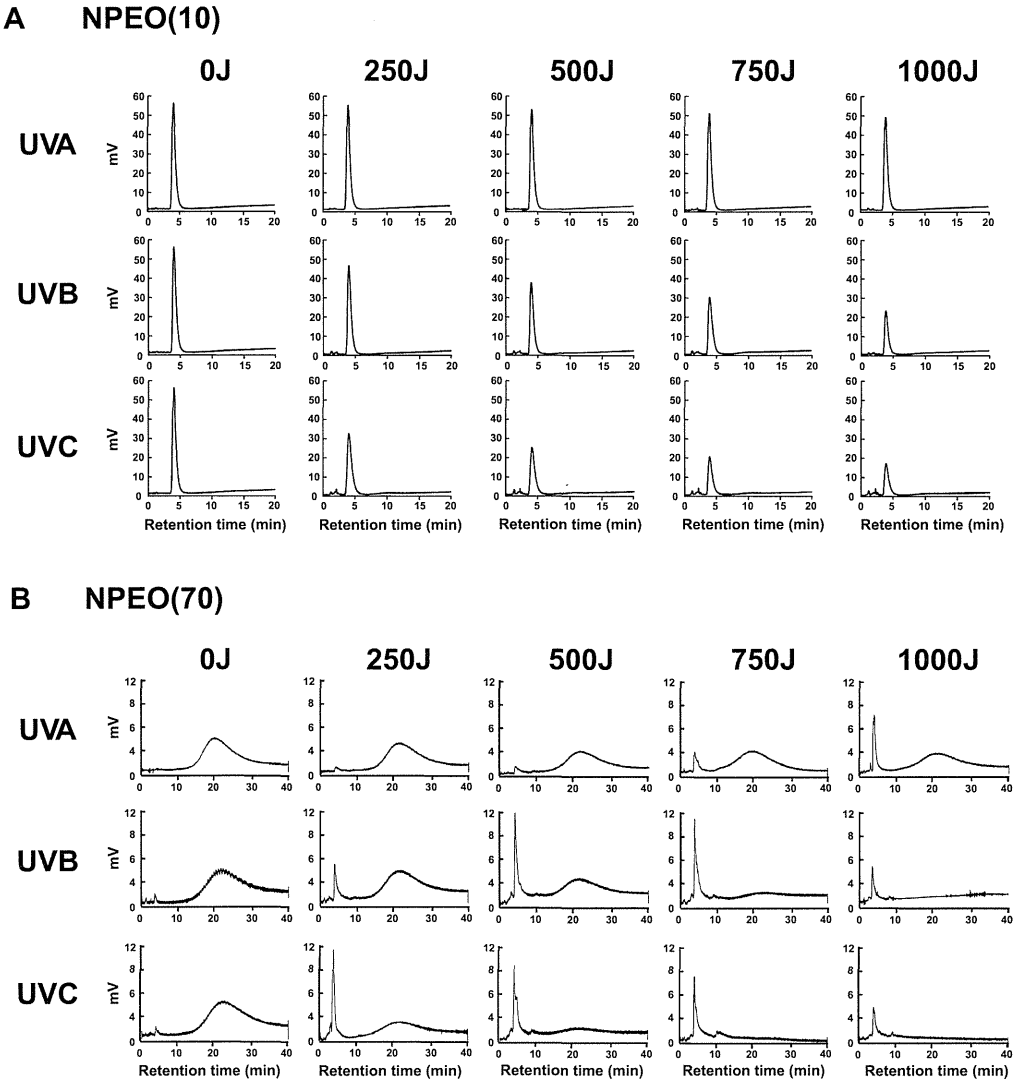

Figure 1. HPLC analysis of UV-irradiated NEPOs. UV (~1000 J cm^{-2})-irradiated NPEO(10) (A) and NPEO(70) (B) were analyzed using HPLC.

with a primary antibody against phospho-H2AX (rabbit polyclonal) (1:1000) or actin (Santa Cruz Biotechnol. CA, 1:1000), then with a secondary antibody conjugated with horseradish peroxidase (Jackson Immuno Research Laboratories, PA) for 1 h. The bands of γ-H2AX were visualized with an enhanced chemiluminescence detection kit (GE Healthcare Ltd. UK).

Flow cytometric analysis of γ-H2AX and cell cycle distribution. The cells treated with UV-irradiated NPEOs were fixed in ice-cold 70% ethanol and kept at −20°C for at least 2 h. The fixed cells were centrifuged at 400 ***g*** rpm for 5 min and washed twice with PBS. They were resuspended in PBS containing 0.2% triton X-100 and 1% BSA (BSA-T-PBS) and kept at room temperature for 15 min. Cells were incubated with phospho-H2AX (mouse monoclonal) (1:200) for 1 h, then with a secondary antibody conjugated with FITC (1:200) (Jackson Immuno Research Laboratories, PA) for 1 h in BSA-T-PBS. After the immunoreaction, the cells were resuspended in BSA-T-PBS containing 1 $\mu g\ mL^{-1}$ RNase A. PI (10 $\mu g\ mL^{-1}$) was added prior to the measurement for the cell cycle analysis. The fluorescence intensity of FITC and PI was determined using flow cytometry (FCM) (FACS CANTTM II; Becton Dickinson, Franklin Lakes, NJ). At least 10 000 cells per sample were analyzed.

Detection of DNA double strand breaks. DSBs were detected with a biased sinusoidal field gel electrophoresis (BSFGE) system (Atto, Japan). The cells treated with UV-irradiated NPEOs were solidified in 1% low-melting agarose. The agarose plugs were treated with proteinase K (0.5 mg mL^{-1}) and ribonuclease A (1 mg mL^{-1}), and electrophoresed in a 0.8% agarose gel. The gel was visualized by staining with ethidium bromide.

All experiments above were repeated two or three times.

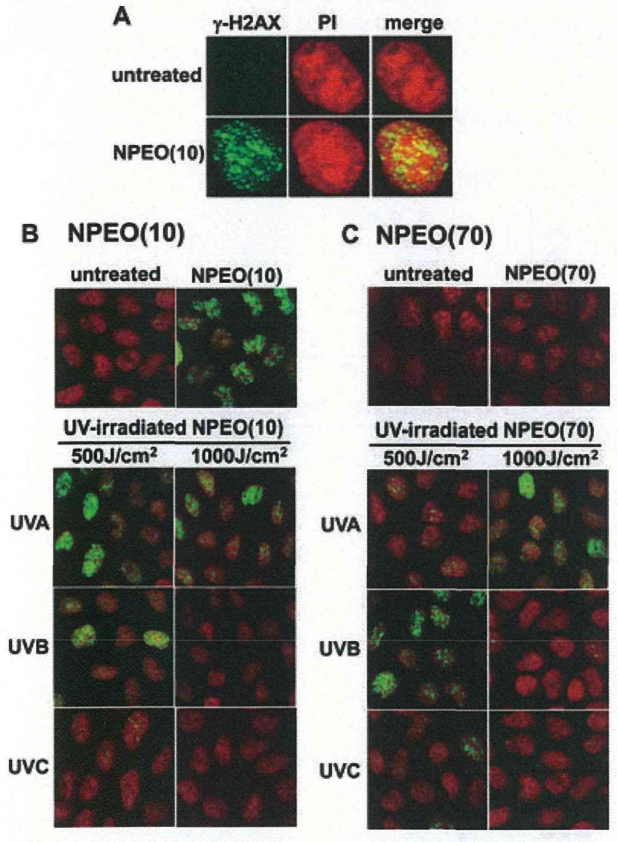

Figure 2. Images of formation of γ-H2AX foci after treatment with UV-irradiated NPEOs. (A) Magnified images of γ-H2AX foci produced by treatment with UV-irradiated NPEO(10) (300 μM) for 4 h. Nuclei were stained with PI. Left panels: γ-H2AX, center panels: nuclei stained by PI, right panels: merged images. (B) γ-H2AX produced by NPEO(10) exposed to UVA, B and C (500 and 1000 J cm^{-2}). (C) γ-H2AX produced by NPEO(70) exposed to UVA, B and C (500 and 1000 J cm^{-2}).

RESULTS

Degradation of NPEOs by UV having different wavelengths

The degradation of NPEO(10) and NPEO(70) after UVA, B and C irradiation was analyzed using HPLC. Each degraded product of NPEO(10) and NPEO(70) was separated on the same HPLC column using a mobile phase buffer of acetonitrile/water as described in Materials and Methods (Fig. 1). The retention times of NPEO(10) and NPEO(70) were 4 min and 20–25 min, respectively. In Fig. 1A, the peak of NPEO(10) became smaller with exposure to UVB and UVC, whereas the degradation induced by UVA was slight.

In Fig. 1B, the peak of NPEO(70) decreased after UV irradiation and the peaks of NPEOs having short side chains (around 10 units long) appeared, which were remarkable after UVB and UVC irradiation. UVA caused some degradation of NPEO(70), which was observed as a decrease in the peak of NPEO(70) and the appearance of a peak of NPEO (around 10). Intermediate peaks between NPEO(10) and (70), for example NPEO(40), did not appear under any UV irradiation. With UVC irradiation at 1000 J cm^{-2}, the peak of NPEO(70) completely disappeared and the peaks of NPEOs having short side chains (around 10 units) also became negligibly small.

Generation of γ-H2AX after treatment with UV-irradiated NPEOs

We recently showed NPEO(10), not NPEO(70), to be genotoxic, using γ-H2AX, a marker of DNA damage (13). The toxicity chan-

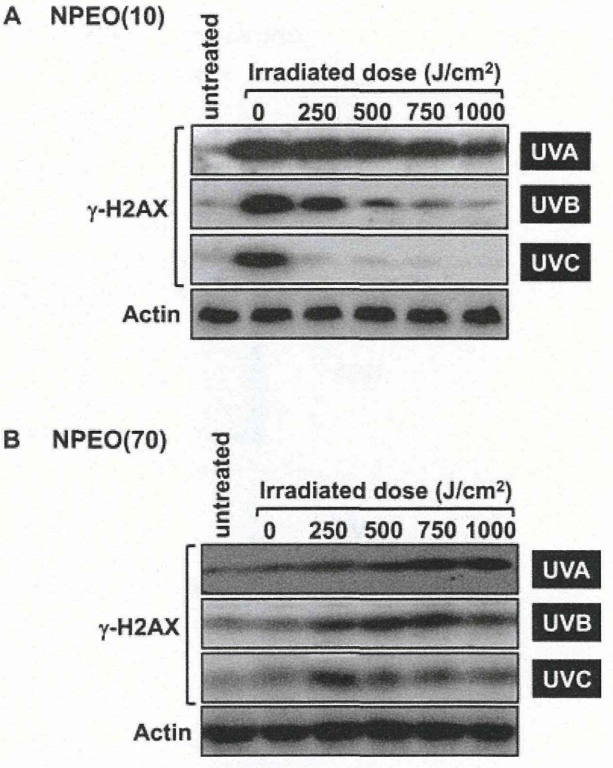

Figure 3. Generation of γ-H2AX after treatment with UV-irradiated NPEOs. γ-H2AX after treatment with UV-irradiated NPEO(10) (A) and NPEO(70) (B) (100 μM) for 4 h was detected using Western blotting. Actin was used as a standard for the equal loading of proteins for SDS-PAGE.

ged with the degradation of EO units by UVB irradiation (12). As NPEOs showed different degradation rates dependent on UV wavelengths, a corresponding change in genotoxic ability was expected. Figure 2A shows images of the γ-H2AX generated by NPEO(10). NPEO(10) produced a remarkable number of γ-H2AX foci in the nucleus. UVB and UVC, but not UVA, decreased the number (Fig. 2B). Conversely, NPEO(70) generated no foci of γ-H2AX until after UV irradiation (Fig. 2C). NPEO(70) exposed to UVB (500 J cm^{-2}) produced γ-H2AX, but that exposed to an excess dose (1000 J cm^{-2}) did not. UVC (250 J cm^{-2}) caused similar levels of γ-H2AX (data not shown) and excess exposure (500 and 1000 J cm^{-2}) gradually decreased the amount. For UVA, 1000 J cm^{-2} was needed for the formation of γ-H2AX foci.

These changes were analyzed in detail by Western blotting (Fig. 3). UVA irradiation only slightly decreased the amount of γ-H2AX generated by NPEO(10) (Fig. 3A). Moreover, 500 J cm^{-2} of UVB and 250 J cm^{-2} of UVC markedly suppressed γ-H2AX production by NPEO(10). With NPEO(70) (Fig. 3B), high doses (750–1000 J cm^{-2}) of UVA and doses of UVB above 250 J cm^{-2} resulted in γ-H2AX production. γ-H2AX was also generated with small doses of UVC, but excess exposure reversed the process. These results were consistent with the results of formation of γ-H2AX foci in Fig. 2.

Cell cycle-dependent generation of γ-H2AX was examined using FCM (Fig. 4). After treatment with NPEO(10), γ-H2AX was formed independently of the cell cycle. The γ-H2AX produced by NPEO(10) disappeared after exposure to UVB and UVC. Conversely, NPEO(70) produced no γ-H2AX in any phase of the cell cycle. UV irradiation caused NPEO(70) to generate γ-H2AX. The generation of γ-H2AX by NPEO(70) exposed to UVA, B and C was independent of the cell cycle.

Formation of DSBs after treatment with UV-irradiated NPEOs

As the generation of γ-H2AX is attributed to the formation of DSBs, DSBs induced by treatment with UV-irradiated NPEO(10) and NPEO(70) for 4 h were detected by BSFGE (Fig. 5). NPEO (10) caused DNA migration, but NPEO(70) did not. UVA irradiation did not influence the migration, whereas UVB and UVC irradiation attenuated it in a dose-dependent manner. Conversely, irradiation caused NPEO(70) to damage DNA, with UVC most effective, then UVB and UVA. These results were consistent with the data for γ-H2AX in Figs. 2–4.

DISCUSSION

UV has been used to degrade several environmental contaminants (26–28). For some chemicals, the degradation process is advanced in the presence of ozone and photocatalysts (28–30). The UV spectrum can be divided into UVA (320–400 nm), UVB (280–320 nm) and UVC (200–280 nm), with the energy ranking in decreasing order: UVC > UVB > UVA. In this study, we found that NPEOs were degraded dependent on the energy of

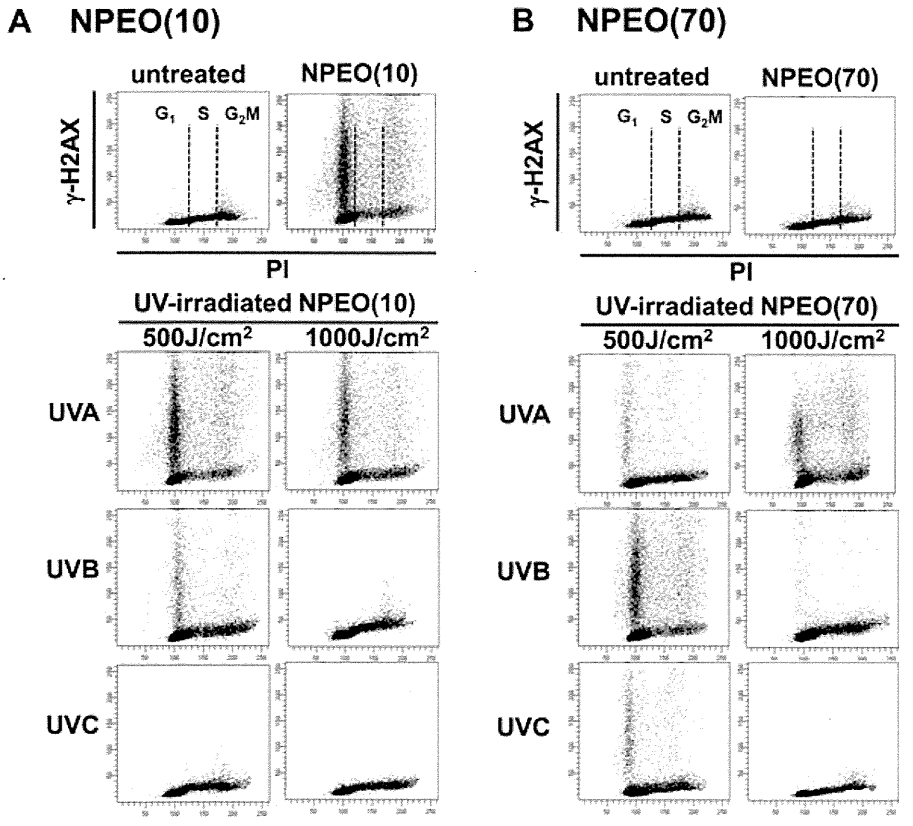

Figure 4. Flow cytometric analysis of γ-H2AX and cell cycle phases after treatment with UV-irradiated NPEOs. Cells treated with NPEOs for 4 h were fixed and immune stained with γ-H2AX antibody and PI as described in Materials and Methods. The cells were analyzed using FCM and cell cycle-dependent formation of γ-H2AX was revealed as dotted blots. (A): NPEO(10), (B): NPEO(70).

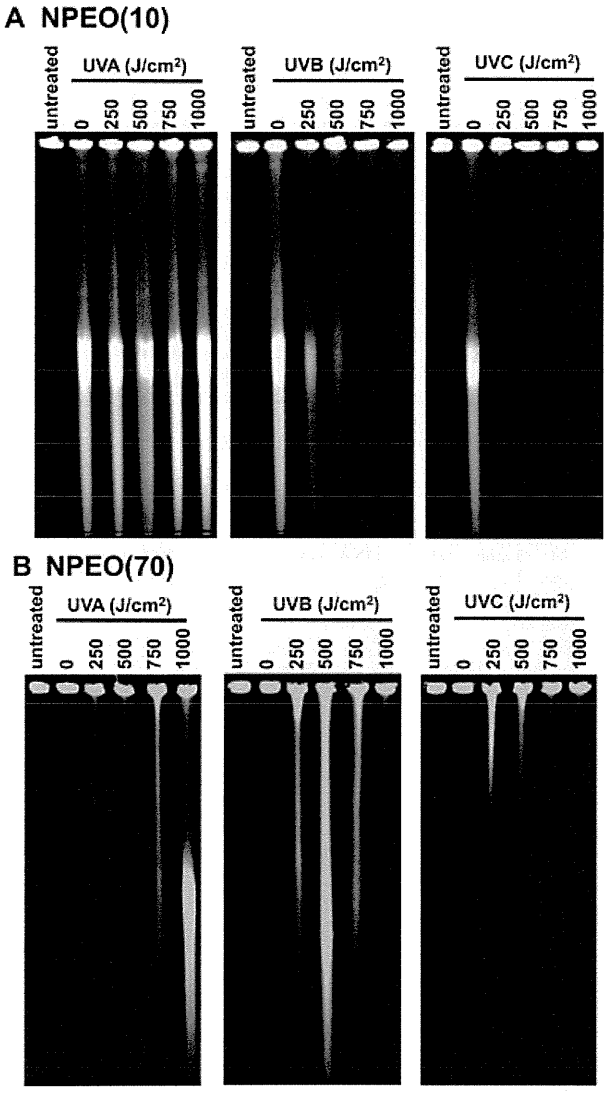

Figure 5. Formation of DSBs after treatment with UV-irradiated NPEOs. Cells treated with NPEOs for 4 h were solidified in 1% low-melting agarose and treated as described in Materials and Methods. The gel stacks containing the cells were loaded onto a 0.8% agarose gel, and BSFGE was carried out. (A): NPEO(10), (B): NPEO(70).

UV, that is, UVC was most effective and UVA caused little change. As the benzene ring in NPEOs absorbs shorter wavebands of UV having high energy, the degradation by UVB and UVC is more effective than that by UVA.

The changes in HPLC patterns following exposure to UVB or UVC suggested the EO side chain to be degraded with the benzene ring. The photolysis of the EO side chain differed between NPEO (10) and (70). This had been found in our previous study using UVB (7), that is, the EO side chain of NPEO(10) was gradually degraded from the end of the EO unit, but that of NPEO(70) was degraded from near the benzene ring. As shown in Supplementary Fig. 1, NPEO(10) lost its side chain, depending on the dose of UVB and C. NPEO(70) was degraded by UVA, B and C, resulting in the production of NPEOs having around 10 EO units, not NPEOs having more EO units (Fig. 1). Ahel *et al.* (31) reported that photochemical degradation of both NPEOs and NP was mainly due to sensitized photolysis and that direct photolysis was slow, in which singlet oxygen was not important. Some reports showed that hydroxyl radicals can react with polyethoxylated chains of alcohol ethoxylates and octylphenol ethoxylates as well as aromatic rings (32,33). We suspected that the reactive oxygen species (ROS) produced following energy absorption of UVB and UVC by benzene rings would attack the EO side chains of NPEOs; however, the exact mechanism was not clarified.

γ-H2AX is currently attracting attention as a new biomarker for detecting genotoxic insults (17,18). Based on γ-H2AX, we recently showed that the genotoxic effect of NPEOs was strongly dependent on the number of EO units and that UVB irradiation drastically changed the genotoxic potential of NPEO(15) and NPEO(70) (12). NPEO(15) showed a great ability to form γ-H2AX, which was reduced by UVB irradiation. Conversely, nongenotoxic NPEO(70) was able to generate γ-H2AX after UVB irradiation. In this study, γ-H2AX production reflected the degradation patterns of NPEO(10) and NPEO(70) according to wavelengths of UV as shown in Fig. 1. Dependent on the energy of UV, the generation of γ-H2AX by NPEO(10) was attenuated, whereas NPEO(70) which has no genotoxicity became able to generate γ-H2AX and excess irradiation made it nongenotoxic again. The patterns of DNA migration detected by BSFGE were almost the same. As γ-H2AX has been considered to be caused by DSBs (16), we confirmed the formation of DSBs by NPEO (10) and degraded NPEO(70). From our previous study, the generation of γ-H2AX by NPEO(15) and NPEO(70) degraded by UVB was independent of the cell cycle (12). γ-H2AX generated by NPEO(10) and NPEO(70) degraded by different wavelengths of UV was also observed throughout the cell cycle (Fig. 4). DNA lesions would later be converted into DSBs as a consequence of the collision of the replication forks. Therefore, if DNA lesions like oxidative bases formed, γ-H2AX would be detected mainly in the S phase (34). This means that NPEO(10) and degraded NPEO(70) did not form γ-H2AX *via* replication stress.

DSBs are a serious form of damage which can lead to cell death and mutation. Cell death patterns were similar with the generation of γ-H2AX and DSBs in Figs. 3–5 (Supplementary Fig. 2). Mistakes in the repair of DSBs may be an important factor in the development of genomic instability (35). At least two mechanisms, homologous recombination (HR) and nonhomologous end joining (NHEJ), are known for the repair of DSBs. Although HR is an error-free repair pathway, NHEJ is an error-prone one. Increased NHEJ misrepair in response to excess DSBs formed by NPEOs and degraded NPEOs could lead to increased genomic instability. Therefore, appearance of genotoxicity in NPEOs with long EO chains after exposure to several wavelengths of UV is important for risk assessment of NPEOs.

In environments, several contaminants with NPEOs would affect degradation. In the absence of contaminants, UVB might be effective for the degradation of NPEOs, whereas in the presence of contaminants, the more permeable UVA might be effective because short wavelengths of UV are easily masked by contaminants; however, selective production of NPEO having short EO chains would be a problem. The intermediates in the degradation of NPEOs by sunlight should receive attention because they could be detrimental to living organisms.

Acknowledgements—This work was supported in part by Grants-in-aid for Young Scientific Research (B) (#22710065) and for Scientific

Research (C) (#24510084) from the Ministry of Education, Culture, Sports, Science and Technology, and for Research on Risk of Chemical Substances from the Ministry of Health, Labor, and Welfare of Japan.

SUPPORTING INFORMATION

Additional Supporting Information may be found in the online version of this article:

Figure S1. HPLC analysis of UV-irradiated NEPO(10). UV (~1000 J cm^{-2})-irradiated NPEO (10) was analyzed using HPLC (mobile phase: *n*-hexane, isopropanol and water). NP and NPEO (6) as standards separated as a single peak, whereas NPEO(10) showed multiple peaks because it was produced for industry and contained NPEOs with slightly different side chain lengths. NP and NPEOs with shorter side chains (~10) appeared after UVB and UVC irradiation, depending on the irradiation dose. The gradual degradation and disappearance of side chains were more remarkable after UVC than UVB irradiation.

Figure S2. Cytotoxicity of NPEOs irradiated with UV. Human fibroblasts, ASF4-1 cells, were treated with NPEO(10) (A) and NPEO(70) (B) irradiated (~1000 J cm^{-2}) at a concentration of 100 μM. Cell survival 24 h after the treatment was determined by alamer Blue™ assay (Diagnostic systems Inc., USA). Values are the mean ± SD (n = 5). $*P < 0.05$, $***P < 0.001$

Please note: Wiley-Blackwell are not responsible for the content or functionality of any supporting materials supplied by the authors. Any queries (other than missing material) should be directed to the corresponding author for the article.

REFERENCES

1. Soares, A., B. Guieysse, B. Jefferson, E. Cartmell and J. N. Lester (2008) Nonylphenol in the environment: A critical review on occurrence, fate, toxicity and treatment in wastewaters. *Environ. Int.* **34**, 1033–1049.
2. Ying, G. G. (2006) Fate, behavior and effects of surfactants and their degradation products in the environment. *Environ. Int.* **32**, 417–431.
3. Sharma, V. K., G. A. Anquandah, R. A. Yngard, H. Kim, J. Fekete, K. Bouzek, A. K. Ray and D. Golovko (2009) Nonylphenol, octylphenol, and bisphenol-A in the aquatic environment: A review on occurrence, fate, and treatment. *J. Environ. Sci. Health A Tox. Hazard Subst. Environ. Eng.* **44**, 423–442.
4. Ying, G. G., B. Williams and R. Kookana (2002) Environmental fate of alkylphenols and alkylphenol ethoxylates–a review. *Environ. Int.* **28**, 215–226.
5. Giger, W., P. H. Brunner and C. Schaffner (1984) 4-Nonylphenol in sewage sludge: Accumulation of toxic metabolites from nonionic surfactants. *Science* **225**, 623–625.
6. Tollefsen, K. E., C. Blikstad, S. Eikvar, E. Farmen Finne and I. Katharina Gregersen (2008) Cytotoxicity of alkylphenols and alkylated non-phenolics in a primary culture of rainbow trout (Onchorhynchus mykiss) hepatocytes. *Ecotoxicol. Environ. Saf.* **69**, 64–73.
7. Goto, R., T. Kubota, Y. Ibuki, K. Kaji and A. Goto (2004) Degradation of nonylphenol polyethoxylates by ultraviolet B irradiation and effects of their products on mammalian cultured cells. *Toxicol.* **202**, 237–247.
8. Neamţu, M. and F. H. Frimmel (2006) Photodegradation of endocrine disrupting chemical nonylphenol by simulated solar UV-irradiation. *Sci. Total Environ.* **369**, 295–306.
9. Chen, L., H. Y. Zhou and Q. Y. Deng (2007) Photolysis of nonylphenol ethoxylates: The determination of the degradation kinetics and the intermediate products. *Chemosphere* **68**, 354–359.
10. Kim, J., J. Park, P. G. Kim, C. Lee, K. Choi and K. Choi (2010) Implication of global environmental changes on chemical toxicity-effect of water temperature, pH, and ultraviolet B irradiation on acute toxicity of several pharmaceuticals in Daphnia magna. *Ecotoxicology* **19**, 662–669.
11. Ohnuki, G., T. Toyooka and Y. Ibuki (2010) UVB in solar-simulated light causes formation of BaP-photoproducts capable of generating phosphorylated histone H2AX. *Mutat. Res.* **702**, 70–77.
12. Toyooka, T., T. Kubota and Y. Ibuki (in press) UVB irradiation changes genotoxic potential of nonylphenol polyethoxylates –remarkable generation of γ-H2AX with degradation of chemical structure. *Mutagenesis*. DOI: 10.1093/mutage/ges043.
13. Toyooka, T., T. Kubota and Y. Ibuki (2012) Nonylphenol polyethoxylates induce phosphorylation of histone H2AX. *Mutat. Res.* **741**, 57–64.
14. Seike, N., H. Wanibuchi, K. Morimura, M. Wei, T. Nishikawa, K. Hirata, J. Yoshikawa and S. Fukushima (2003) Enhancement of lung carcinogenesis by nonylphenol and genistein in a F344 rat multiorgan carcinogenesis model. *Cancer Lett.* **192**, 25–36.
15. Fukamachi, K., B. S. Han, C. K. Kim, N. Takasuka, Y. Matsuoka, E. Matsuda, T. Yamasaki and H. Tsuda (2004) Possible enhancing effects of atrazine and nonylphenol on 7,12-dimethylbenz[a]anthracene-induced mammary tumor development in human c-Ha-ras proto-oncogene transgenic rats. *Cancer Sci.* **95**, 404–410.
16. Rogakou, E. P., D. R. Pilch, A. H. Orr, V. S. Ivanova and W. M. Bonner (1998) DNA double-stranded breaks induce histone H2AX phosphorylation on serine 139. *J. Biol. Chem.* **273**, 5858–5868.
17. Bonner, W. M., C. E. Redon, J. S. Dickey, A. J. Nakamura, O. A. Sedelnikova, S. Solier and Y. Pommier (2008) GammaH2AX and cancer. *Nat. Rev. Cancer* **8**, 957–967.
18. Mah, L. J., A. El-Osta and T. C. Karagiannis (2010) gammaH2AX: A sensitive molecular marker of DNA damage and repair. *Leukemia* **24**, 679–686.
19. Toyooka, T. and Y. Ibuki (2009) Cigarette sidestream smoke induces phosphorylated histone H2AX. *Mutat. Res.* **676**, 34–40.
20. Ishihama, M., T. Toyooka and Y. Ibuki (2008) Generation of phosphorylated histone H2AX by benzene metabolites. *Toxicol. In Vitro* **22**, 1861–1868.
21. Ibuki, Y., Y. Tani and T. Toyooka (2008) UVB-exposed chlorinated bisphenol a generates phosphorylated histone H2AX in human skin cells. *Chem. Res. Toxicol.* **21**, 1770–1776.
22. Toyooka, T., G. Ohnuki and Y. Ibuki (2008) Solar-simulated light-exposed benzo[a]pyrene induces phosphorylation of histone H2AX. *Mutat. Res.* **650**, 132–139.
23. Toyooka, T. and Y. Ibuki (2006) New method for testing phototoxicity of polycyclic aromatic hydrocarbons. *Environ. Sci. Technol.* **40**, 3603–3608.
24. Toyooka, T., M. Ishihama and Y. Ibuki (2011) Phosphorylation of histone H2AX is a powerful tool for detecting chemical photogenotoxicity. *J. Invest. Dermatol.* **131**, 1313–1321.
25. Ibuki, Y. and R. Goto (2002) Antiapoptotic effects induced by different wavelengths of ultraviolet light. *Photochem. Photobiol.* **75**, 495–502.
26. Chen, C., S. Yang, Y. Guo, C. Sun, C. Gua and B. Xu (2009) Photolytic destruction of endocrine disruptor atrazine in aqueous solution under UV irradiation: Products and pathways. *J. Hazard. Materials* **172**, 675–684.
27. Poster, D. L., M. Chaychian, P. Neta, R. E. Huie, J. Silverman and M. Al-Sheikhly (2003) Degradation of PCBs in a marine sediment treated with ionizing and UV radiation. *Environ. Sci. Technol.* **37**, 3808–3815.
28. Lau, T. K., W. Chu and N. Graham (2007) Reaction pathways and kinetics of butylated hydroxyanisole with UV, ozonation, and UV/O_3 processes. *Water Res.*, **41**(4), 765–774.
29. Zhang, Y. and J. L. Zhou (2008) Occurrence and removal of endocrine disrupting chemicals in wastewater. *Chemosphere* **73**, 848–853.
30. Sin, J. C., S. M. Lam, A. R. Mohamed and K. T. Lee (2012) Degrading endocrine disrupting chemicals from wastewater by TiO (2) photocatalysis: A review. *Int. J. Photoenergy* 185159. 23 pp. DOI: 10.1155/2012/185159.
31. Ahel, M., F. E. Scully, J. Hoigne and W. Giger (1994) Photochemical degradation of nonylphenol and nonylphenol polyethoxylates in natural waters. *Chemosphere* **28**, 1361–1368.

32. Brand, N., G. Mailhot and M. Bolte (2000) The interaction "light, Fe(III)" as a tool for pollutant removal in aqueous solution: Degradation of alcohol ethoxylates. *Chemosphere* **40**, 395–401.
33. Liu, G., S. Zheng, X. Xing, Y. Li, D. Yin, Y. Ding and W. Pang (2010) Fe(III)-oxalate complexes mediated photolysis of aqueous alkylphenol ethoxylates under simulated sunlight conditions. *Chemosphere* **78**, 402–408.
34. Tanaka, T., X. Huang, H. D. Halicka, H. Zhao, F. Traganos, A. P. Albino, W. Dai and Z. Darzynkiewicz (2007) Cytometry of ATM activation and histone H2AX phosphorylation to estimate extent of DNA damage induced by exogenous agents. *Cytometry A.* **71**, 648–661.
35. Rassool, F. V., T. J. Gaymes, N. Omidvar, N. Brady, S. Beurlet, M. Pla, M. Reboul, N. Lea, C. Chomienne, N. S. Thomas, G. J. Mufti and R. A. Padua (2007) Reactive oxygen species, DNA damage, and error-prone repair: A model for genomic instability with progression in myeloid leukemia? *Cancer Res.* **67**, 8762–8771.

J Toxicol Pathol 2014; 27: 43–49

Original Article

Establishment of an Invasive Prostate Cancer Model in Transgenic Rats by Intermittent Testosterone Administration

Shinya Sato[1], Shugo Suzuki[1], Aya Naiki-Ito[1], Masami Komiya[1, #], Ne Long[1, ##], Hiroyuki Kato[1], Hiroyuki Sagawa[1], Yoriko Yamashita[1], Tomoyuki Shirai[1, ###], and Satoru Takahashi[1*]

[1] Department of Experimental Pathology and Tumor Biology, Nagoya City University Graduate School of Medical Sciences, 1 Kawasumi, Mizuho-cho, Mizuho-ku, Nagoya 467-8601, Japan
Present: [#] Division of Cancer Prevention Research, National Cancer Center Research Institute, 5-1-1 Tsukiji, Chuo-ku, Tokyo 104-01045, Japan
Present: [##] National Center for Geriatrics and Gerontology, 35 Gengo, Morioka-machi, Obu-city, Aichi, Japan
Present: [###] Nagoya City Rehabilitation Center, 1-2 Mikanyama, Yatomi-cho, Mizuho-ku, Nagoya, Japan

Abstract: We have established a transgenic rat for adenocarcinoma of the prostate (TRAP) model that features uniform adenocarcinoma development in prostatic lobes at high incidence within a short experimental period. However, no invasive carcinomas with reactive stroma characteristics similar to those in man were observed. We therefore have focused on a new model for invasive carcinoma of the prostate using TRAP rats. In experiment 1, male TRAP rats in groups 1 and 2 were treated with orchiectomy at day 0 of the experiment. Rats in groups 1–3 underwent testosterone propionate (TP) implantation from weeks 1 to 4 and from weeks 6 to 16. Rats in groups 1 and 3 were given 3,2'-dimethyl-4-aminobiphenyl (DMAB) after TP implantation. The rats of group 4 served as controls. In experiment 2, the rats were divided into three groups, none of which received DMAB or orchiectomy, treated with TP continuously or with the treatment withdrawn once or twice. In experiment 1, invasive adenocarcinomas with abundant collagenous stroma were found in the dorsolateral and anterior prostate, some of which showed perineural space invasion at week 16. The number of invasive carcinoma foci was most frequent in group 3. In experiment 2, invasive adenocarcinoma development in the lateral prostates was correlated with the number of TP administration/withdrawal cycles. In conclusion, our newly established rat model for invasive adenocarcinoma of the prostate could serve as a useful preclinical model for evaluating the *in vivo* efficacy of preventive and therapeutic agents targeting of the tumor microenvironment. (DOI: 10.1293/tox.27.2013-0052; J Toxicol Pathol 2014; 27: 43–49)

Key words: prostate cancer, animal model, cancer invasion, transgenic rat, testosterone propionate, intermittent administration

Introduction

Prostate cancer is the most common cancer and the second leading cause of death from cancer among men in the US. It has been estimated there will be approximately 238,590 new cases of prostate cancer and 29,720 deaths from prostate cancer in the US in 2013[1]. In Japan, the prevalence and mortality of prostate cancer has also been increasing, along with in the so-called nutrition transition[2, 3]. Androgen ablation therapy is generally applied for prostate cancer because of hormone-dependent growth. However, outgrowth of androgen-independent and metastatic cancer cells is a frequent outcome, eventually leading to death of the patient. Therefore, understanding of the mechanisms of the acquisition of metastatic potential or the androgen-independent phenotype of cancer cells is urgently required.

We have established a rat cancer model responding to the need for *in vivo* systems that adequately reproduce the spectrum of human prostate cancers. Administration of 3,2'-dimethyl-4-aminobiphenyl (DMAB) induces noninvasive and androgen-dependent adenocarcinomas in the ventral prostate, while additional long-term treatment with testosterone propionate (TP) causes development of invasive and metastasizing androgen-independent adenocarcinomas arising from the dorsolateral and anterior prostate and seminal vesicles[4, 5]. However, a long period of about 60 weeks is required to induce prostate cancers in both carcinogenesis models, and the incidence of lesion development is relatively low. Therefore, we have established transgenic rats bearing a probasin promoter/simian virus 40 (SV40) T antigen construct to resolve these problems[6]. This model, the transgenic rat for adenocarcinoma of the prostate (TRAP), features development of high-grade prostatic intraepithelial neoplasia (HGPIN) from 4 weeks of age and androgen-dependent well-moderately differentiated adenocarcinomas with 100% incidences by the age of 15 weeks. These

Received: 8 September 2013, Accepted: 28 October 2013
*Corresponding author: S Takahashi (e-mail: sattak@med.nagoya-cu.ac.jp)

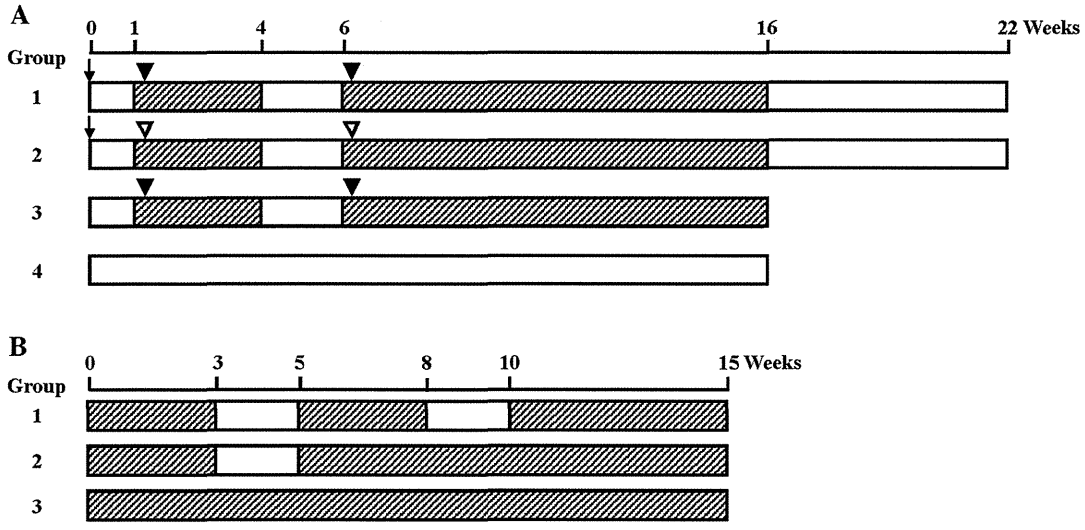

Fig. 1. Experimental design for experiments 1 (A) and 2 (B) for induction of invasive prostate adenocarcinomas in TRAP rats. The animals used were male TRAP rats that were 6 weeks of age at commencement of the study. Shaded, testosterone propionate, silicone rubber tube (40 mg); arrow, bilateral orchiectomy; filled arrowhead, DMAB 50 mg/kg b.w.; open arrowhead, vehicle (corn oil).

characteristics of the TRAP model have been shown to be very suitable for evaluation of strategies for chemoprevention and treatment[7–10]. Microinvasive carcinomas characterized by a budding morphology from acini are observed in an age-dependent manner in TRAP rats, but these lesions are generally only 0.2–0.3 mm diameter in size and take over 35 weeks to develop[11]. We speculated that testosterone administration might be of paramount importance in the induction of invasive carcinoma in our transgenic rats based on our experience with the DMAB combined with TP-induced prostate carcinogenesis model. In the present study, we therefore assessed whether testosterone exposure might result in a high-grade invasive phenotype or metastatic lesions in TRAP rats.

Materials and Methods

Chemicals

TP was purchased from Sigma-Aldrich (St. Louis, MO, USA) and DMAB was obtained from Matsugaki Pharmaceutical Co. (Osaka, Japan). The purity of DMAB was >98%. Antibody for androgen receptor (AR) was obtained from Santa Cruz Biotechnology Inc (N-20, Santa Cruz, CA, USA). The antibody for Ki-67 was from Acris Antibodies GmbH (SP-6, Hiddenhausen, Germany).

Animals

Male heterozygous TRAP rats with a Sprague–Dawley genetic background were obtained from Oriental BioService Inc. (Minamiyamashiro, Kyoto, Japan) and were housed in plastic cages with hardwood chips in an air-conditioned room with a 12 h light/dark cycle at 23 ± 2°C and 50 ± 10% humidity. Food (Oriental MF; Oriental Yeast Co., Ltd., Tokyo, Japan) and tap water were available *ad libitum*. They were acclimatized for 1 week before use. Surgical treatments, such as orchiectomy and tube implantation, were carried out under deep isoflurane anesthesia. All animal experiments were performed under protocols approved by the Institutional Animal Care and Use Committee of the Nagoya City University Graduate School of Medical Sciences.

Experimental protocols

Experiment 1: A total of 24 male TRAP rats aged 6 weeks were randomly divided into four groups. Rats in groups 1 and 2 were treated with bilateral orchiectomy at day 0 of the experiment. Those in groups 1–3 underwent subcutaneous implantation of 2-cm-long silicone rubber tubes (Silascon®, inner diameter, 0.2 cm; outer diameter, 0.3 cm, Kaneka Medix Corporation, Osaka, Japan) containing 40 mg TP sealed at both ends with silicone rubber sealing compound (KE-42, Shin-Etsu Chemical Co., Ltd., Tokyo, Japan) into the interscapular region from weeks 1 to 4 and from weeks 6 to 16. The TP implants were replaced at 6-week intervals. Rats in groups 1 and 3 were subcutaneously given DMAB at a dose of 50 mg/kg body weight on the second day after TP tube implantation. No treatment was performed in rats of group 4, which served as controls. Animals were euthanized at weeks 16 and 22 after the beginning of the experiment (Fig.1A).

Experiment 2: A total of 24 heterozygous male TRAP rats aged 6 weeks were randomly divided into three groups. All were given TP implants in the same manner as in experiment 1 at day 0. The duration of TP administration was different among the groups; that is, TP was administered in experimental weeks 0–3, 5–8 and 10–15 in group 1 and in experimental weeks 0–3 and 5–15 in group 2. Group 3

was continuously administered TP by implants throughout the experiment. The experiment was terminated at week 15 (Fig. 1B).

In both experiments, blood samples were collected from the abdominal aorta under deep anesthesia, and prostates were removed and fixed in formalin. For tissue preparation of prostate glands, four sagittal slices of the ventral prostate, two sagittal samples of the dorsolateral prostate including the urethra, and two transverse slices from each side of the anterior prostate including seminal vesicles were embedded in paraffin. Tissues were processed routinely and stained with hematoxylin and eosin for histopathological examination. Testosterone and estradiol levels in serum were analyzed using radioimmunoassays by a commercial laboratory (SRL, Inc., Tokyo, Japan).

Immunohistochemistry

Deparaffinized sections were incubated with diluted antibodies for AR and Ki-67. The immunohistochemical analysis was performed with a Discovery XT System (Ventana Medical Systems, Tucson, AZ, USA). Incubation with primary antibodies was carried out for 3 hours followed by a one hour incubation with biotinylated anti-rabbit secondary antibody (Vectastain ABC Kit Rabbit IgG, Vector Laboratories, Burlingame, CA, USA) and a DAB detection kit (Ventana Medical Systems) according to the manufacturer's instructions. Sections were counterstained with hematoxylin to facilitate orientation.

Immunofluorescence

Deparaffinized sections were autoclaved at 120°C for 20 min in antigen retrieval solution (Nichirei Biosciences Inc.) and then allowed to cool. Sections were incubated with 1% skim milk for 1 hour at room temperature. For double staining, anti-smooth muscle actin antibodies (1A4, dilution 1:1,000, mouse monoclonal, Dako) and anti-vimentin antibodies (EPR3776, dilution 1:400, rabbit monoclonal, Abcam) were simultaneously added to the slides and incubated for 1 hour at room temperature. After washing the slides with PBS, fluorescein-labeled goat anti mouse IgG (Life Technologies Corporation.) and tetramethylrhodamine-labeled goat anti-rabbit IgG (Life Technologies Corporation.) were added followed by incubation at room temperature for 1 hour. After washing the slides with PBS, the sections were mounted with Vectashield containing DAPI (Vector Laboratories) and subjected to fluorescence microscopy.

Results

Experiment 1

At week 16, foci of invasive adenocarcinoma with abundant collagenous stroma were found in lateral, dorsal and anterior prostates of groups 1–3 (Fig. 2A, B, D, E), along with minute ventral invasive carcinomas with minimal fibrous stroma. Cancer invasion into perineural spaces was also observed (Fig. 2E). Almost all of infiltrating carcinoma cells expressed AR (Fig. 2C, F). The incidences of invasive adenocarcinoma varied among the groups, tending to be higher in group 3 in all prostatic lobes (Table 1). Similarly, the number of invasive carcinoma foci was highest in group 3 (Table 1). There were no differences in histopathological characteristics of invasive adenocarcinomas among the groups. Development of small cell carcinomas of the prostate was sporadically noted, but there were no differences in incidence among the groups. No metastasis of cancer lesions to distant organs was found in any of the groups. Noninvasive adenocarcinomas in the ventral, lateral prostates were observed in all rats of groups 1–4.

At week 22, neoplastic lesions of the prostates were completely resolved with massive involution in all rats of groups 1 and 2. This indicated that all of the invasive adenocarcinomas developed in prostate glands were androgen-dependent (data not shown).

Experiment 2

The results of experiment 1 indicated that bilateral orchiectomy or DMAB administration did not deeply contribute to efficient induction of invasive adenocarcinomas. Thus, we focused on whether TP administration/withdrawal was important.

A significant increase of invasive adenocarcinoma development was observed in group 1, and this correlated well with the number of TP administration/withdrawal cycles in the lateral prostates (Table 2). Multicentric development of invasive adenocarcinoma foci with abundant collagenous stroma was found (Fig. 3A–D), and invasive cancer cells were observed in the stroma (Fig. 3E) and were positive for AR protein (Fig. 3F). Some invasive lesions consisted of cells with atrophic features, but more than 50% of these cells were labeled for Ki-67, suggesting that they were high-grade adenocarcinomas (Fig. 3G). Reactive stromal cells surrounding invasive cancers expressed both smooth muscle actin and vimentin and were therefore revealed to be cancer-associated myofibroblasts (Fig. 4). Noninvasive adenocarcinomas in the ventral and lateral prostates were found in all rats of groups 1–3.

Discussion

The TRAP rat features sequential progression from prostatic intraepithelial neoplasias (PINs) to noninvasive adenocarcinomas through prostate epithelial cell-specific expression of the SV40 T antigen regulated by the androgen-dependent probasin promoter. We have applied the TRAP rat model to validate the chemopreventive effects of a variety of chemicals, and cancer development in TRAP rats is very sensitive to chemicals that modulate the AR axis, such as flutamide, finasteride, resveratrol or angiotensin II receptor blockers [7, 9, 12]. These characteristics underly its acceptability to mimic early-stage hormone naïve human prostate cancer without an invasive phenotype.

In the present study, we established a novel rat model for invasive adenocarcinoma of the prostate in TRAP rats by intermittent TP administration (group 1 in experiment 2,

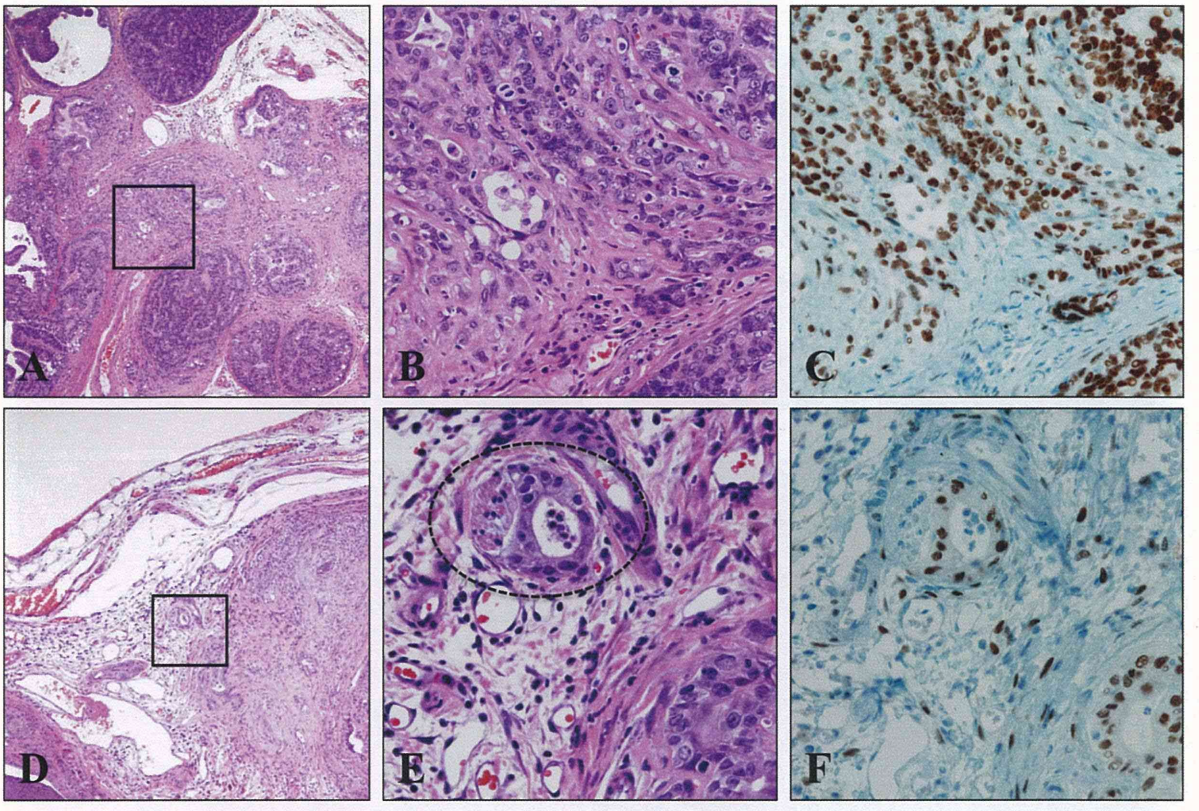

Fig. 2. Representative histopathological findings of invasive adenocarcinomas of the lateral prostate in group 3 (A–C) and anterior prostate in group 2 (D–F). Low (A, D) and high (B, E) magnifications of lateral and anterior prostates at week 16 after after the beginning of experiment 1. The rectangles in (A) and (D) represent the areas from (B) and (E), respectively. The dotted circle in (E) indicates perineural cancer invasion. (C, F) AR immunohistochemistry.

Table 1. Incidence and Multiplicity of Invasive Adenocarcinoma (at Week 16, Experiment 1)

Group	No. of rats	Ventral		Lateral		Dorsal		Anterior	
		Incidence (%)	No. of foci	Incidence (%)	No. of foci	Incidence (%)	No. of foci	Incidence (%)	No. of foci
1	5	1 (20)	0.20 ± 0.45	4 (80)	1.80 ± 1.64	1 (20)	0.20 ± 0.45	3 (60)	0.80 ± 0.84
2	4	2 (50)	1.00 ± 1.15	3 (75)	3.75 ± 3.78	1 (25)	0.25 ± 0.50	3 (75)	2.75 ± 3.10
3	4	4 (100)	4.00 ± 1.41[a,b]	4 (100)	6.00 ± 2.45[c]	3 (75)	1.00 ± 0.82	4 (100)	2.00 ± 0.82
4	5	2 (40)	0.40 ± 0.55	1 (20)	0.20 ± 0.45	0	-	2 (40)	0.40 ± 0.55

[a] $P<0.001$ vs groups 1 and 4; [b] $P<0.01$ vs group 2; [c] $P<0.05$ vs group.

Table 2. Incidence and Multiplicity of Invasive Adenocarcinoma (Experiment 2)

Group	No. of rats	Ventral		Lateral		Dorsal		Anterior	
		Incidence (%)	No. of foci	Incidence (%)	No. of foci	Incidence (%)	No. of foci	Incidence (%)	No. of foci
1	9	8 (89)	1.78 ± 1.10	8 (89)	4.22 ± 2.59**	2 (22)	0.44 ± 1.01	6 (67)	1.11 ± 1.05
2	9	7 (78)	1.67 ± 1.41	5 (56)	0.89 ± 0.93	0	-	7 (78)	0.78 ± 0.44
3	6	5 (83)	3.17 ± 1.72	2 (33)	0.33 ± 0.52	0	-	1 (17)	0.17 ± 0.41

** $P<0.01$ vs groups 2 and 3.

shown in Fig. 1). The invasive carcinomas induced simulate human prostate cancer in several respects, such as perineural invasion and multicentric lesion development. To investigate mechanisms of prostate cancer progression, we previously combined administration of both DMAB and TP[5]. While several experiments were conducted with the aim of increasing the incidence of invasive cancer and shortening the experimental period, none exceeded the DMAB + TP

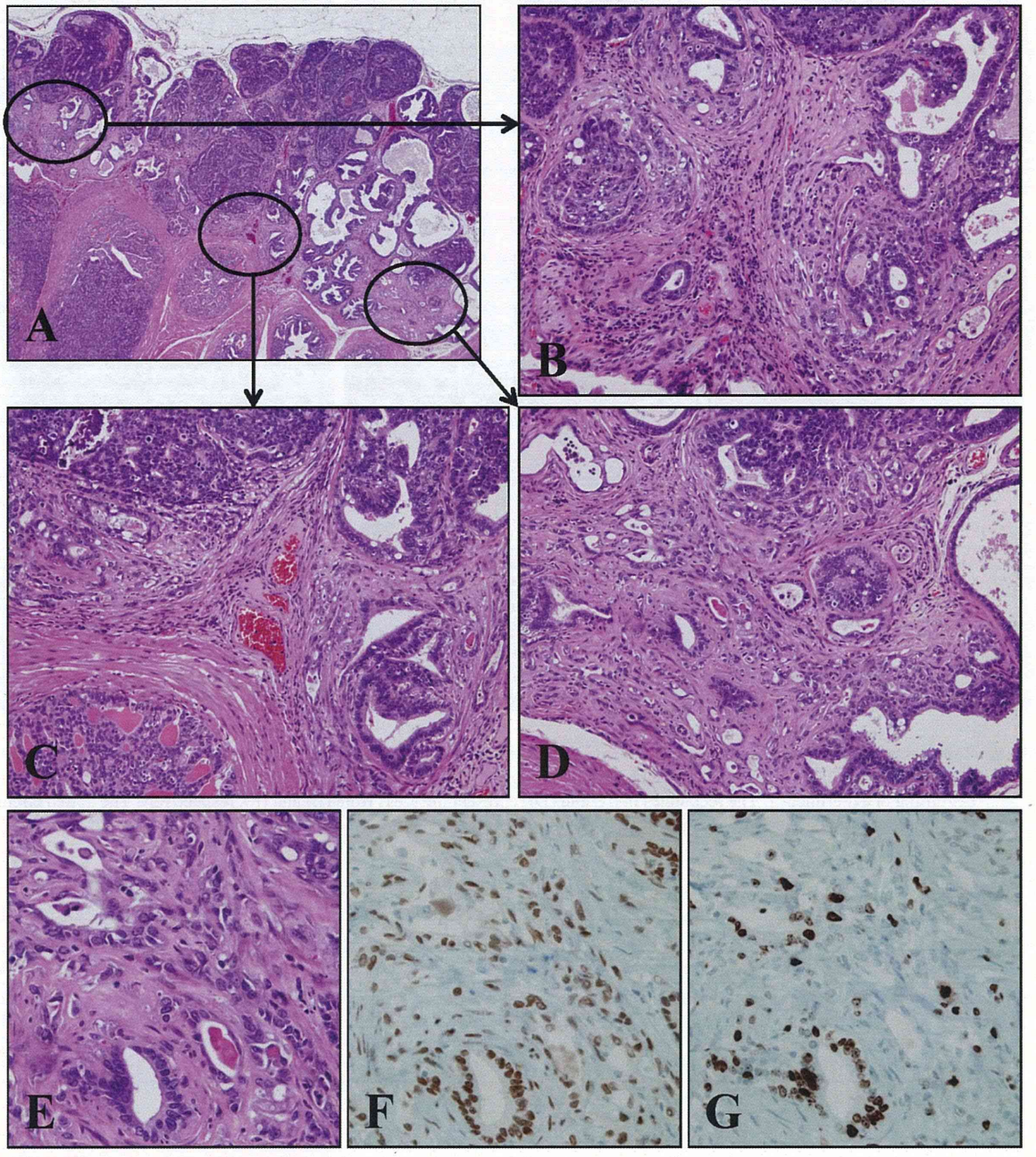

Fig. 3. Multicentric development of invasive adenocarcinomas in the lateral prostate in group 1 at week 15 after the beginning of experiment 2 (A–D). High magnifications of invasive adenocarcinoma with H&E (E), AR (F) and Ki-67 (G) staining.

model in terms of the cancer incidence[13–16]. The new prostate carcinogenesis model documented here is characterized by invasive adenocarcinoma development at a high incidence in a short period without carcinogen administration. This rat model should enable us to investigate candidate chemopreventive agents for therapeutic effects as well as chemopreventive properties against prostate cancer.

We found that invasive adenocarcinoma incidences became greater as we increased the TP administration/withdrawal cycles for the TRAP rats. In our previous studies, testosterone induced invasive prostate adenocarcinomas in a dose- or duration-dependent manner after prostatic carcinogen treatment[14, 15]. However, continuous administration of testosterone alone earlier proved unable to cause development of invasive cancer with abundant reactive stromal tissue in the TRAP model[6,11]. The present results thus lead us to speculate that physiological destruction of the normal acinar structure with stromal cell proliferation by androgen

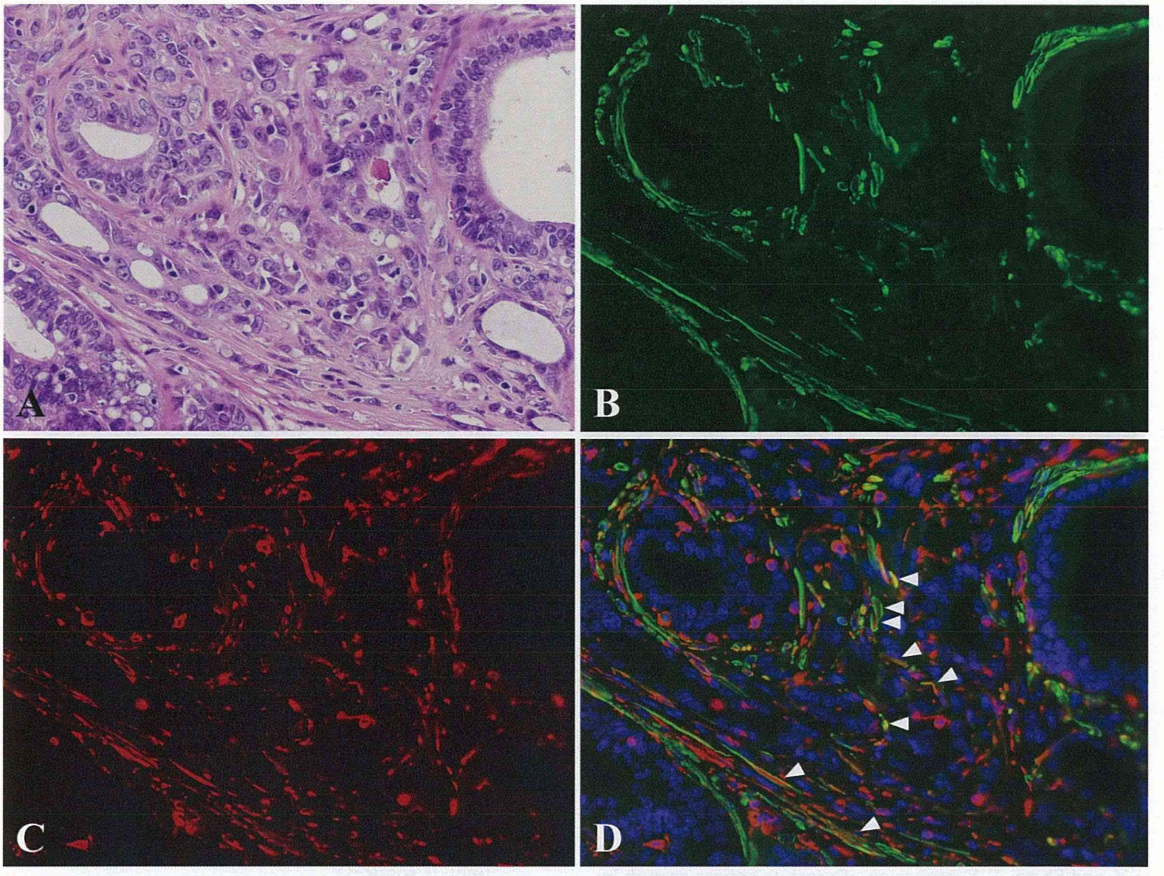

Fig. 4. Immunofluorescence analysis of an invasive adenocarcinoma in a lateral prostate. H&E (A). Immunofluorescence for smooth muscle actin (green, B) and vimentin (red, C), and a merged image (D). Blue, DAPI. Myofibroblasts coexpressing smooth muscle actin and vimentin are indicated by the arrowhead in (D).

depletion plays an important role in the induction of invasive adenocarcinomas.

The process of primary cancer invasion, which initiates metastasis, is multifactorial and multistep and requires alteration of cell adherence, proteolytic degradation of extracellular matrix elements and tumor cell migration through tissue. Accumulating evidence has shown that stromal-epithelial interactions play critical roles in cancer progression[17–19]. The reactive tumor stroma mainly composed of cancer-associated fibroblasts (CAFs) including myofibroblasts, which are the predominant subpopulation of CAFs, is known to contribute to cancer development and progression[18–20]. Growth of myofibroblasts is reported to be stimulated by androgen[21]. TGFβ is one of the growth factors overexpressed in the prostate of rats after androgen ablation by orchiectomy[22]. TGFβ1 induces reactive oxygen species production via enhancement of NOX4 expression and may underly fibroblast-to-myofibroblast differentiation in the prostatic stroma[23], while myofibroblasts per se contribute to the production and activation of TGFβ1 and stromal cell-derived factor-1 (SDF-1)/CXCL12 by autocrine signaling loops[24]. Phosphoglycerate kinase-1 (PGK1), a downstream molecule of CXCL12-CXCR4 signaling, is upregulated in myofibroblasts, and this is involved in the enhanced proliferation and invasion of prostate cancer cells through activation of MMP, AKT and ERK pathways[25].

In conclusion, TP administration/withdrawal cycles appear to be of paramount importance to induction of invasive adenocarcinomas in the TRAP rat prostate. Our new rat prostate carcinogenesis model for invasive adenocarcinoma should provide opportunities to investigate molecular mechanisms of prostate cancer progression and may serve as a useful preclinical model for evaluating *in vivo* efficacy of preventive and therapeutic agents in terms of the tumor microenvironment.

Disclosure statement: The authors have no conflicts of interest.

Acknowledgments: This work was supported by a Grant-in-Aid for Cancer Research from the Ministry of Health, Labour and Welfare of Japan and a grant from the Society for Promotion of Pathology of Nagoya, Japan. The authors have no conflicts of interest regarding this research.

References

1. Siegel R, Naishadham D, and Jemal A. Cancer statistics, 2013. CA Cancer J Clin. **63**: 11–30. 2013. [Medline] [CrossRef]
2. Matsuda T, Marugame T, Kamo K, Katanoda K, Ajiki W, and Sobue T. Cancer incidence and incidence rates in Japan in 2006: Based on data from 15 population-based cancer registries in the monitoring of cancer incidence in Japan (MCIJ) project. Jpn J Clin Oncol. **42**: 139–147. 2012. [Medline] [CrossRef]
3. Zhang J, Dhakal IB, Zhao Z, and Li L. Trends in mortality from cancers of the breast, colon, prostate, esophagus, and stomach in East Asia: role of nutrition transition. Eur J Cancer Prev. **21**: 480–489. 2012. [Medline] [CrossRef]
4. Shirai T, Fukushima S, Ikawa E, Tagawa Y, and Ito N. Induction of prostate carcinoma in situ at high incidence in F344 rats by a combination of 3,2'-dimethyl-4-aminobiphenyl and ethinyl estradiol. Cancer Res. **46**: 6423–6426. 1986. [Medline]
5. Shirai T, Tamano S, Kato T, Iwasaki S, Takahashi S, and Ito N. Induction of invasive carcinomas in the accessory sex organs other than the ventral prostate of rats given 3,2'-dimethyl-4-aminobiphenyl and testosterone propionate. Cancer Res. **51**: 1264–1269. 1991. [Medline]
6. Asamoto M, Hokaiwado N, Cho YM, Takahashi S, Ikeda Y, Imaida K, and Shirai T. Prostate carcinomas developing in transgenic rats with SV40 T antigen expression under probasin promoter control are strictly androgen dependent. Cancer Res. **61**: 4693–4700. 2001. [Medline]
7. Seeni A, Takahashi S, Takeshita K, Tang M, Sugiura S, Sato SY, and Shirai T. Suppression of prostate cancer growth by resveratrol in the transgenic rat for adenocarcinoma of prostate (TRAP) model. Asian Pac J Cancer Prev. **9**: 7–14. 2008. [Medline]
8. Takahashi S, Takeshita K, Seeni A, Sugiura S, Tang M, Sato SY, Kuriyama H, Nakadate M, Abe K, Maeno Y, Nagao M, and Shirai T. Suppression of prostate cancer in a transgenic rat model via gamma-tocopherol activation of caspase signaling. Prostate. **69**: 644–651. 2009. [Medline] [CrossRef]
9. Takahashi S, Uemura H, Seeni A, Tang M, Komiya M, Long N, Ishiguro H, Kubota Y, and Shirai T. Therapeutic targeting of angiotensin II receptor type 1 to regulate androgen receptor in prostate cancer. Prostate. **72**: 1559–1572. 2012. [Medline] [CrossRef]
10. Long N, Suzuki S, Sato S, Naiki-Ito A, Sakatani K, Shirai T, and Takahashi S. Purple corn color inhibition of prostate carcinogenesis by targeting cell growth pathways. Cancer Sci. **104**: 298–303. 2013. [Medline] [CrossRef]
11. Cho YM, Takahashi S, Asamoto M, Suzuki S, Inaguma S, Hokaiwado N, and Shirai T. Age-dependent histopathological findings in the prostate of probasin/SV40 T antigen transgenic rats: lack of influence of carcinogen or testosterone treatment. Cancer Sci. **94**: 153–157. 2003. [Medline] [CrossRef]
12. Cho YM, Takahashi S, Asamoto M, Suzuki S, Tang M, and Shirai T. Suppressive effects of antiandrogens, finasteride and flutamide on development of prostatic lesions in a transgenic rat model. Prostate Cancer Prostatic Dis. **10**: 378–383. 2007. [Medline] [CrossRef]
13. Shirai T, Imaida K, Masui T, Iwasaki S, Mori T, Kato T, and Ito N. Effects of testosterone, dihydrotestosterone and estrogen on 3,2'-dimethyl-4-aminobiphenyl-induced rat prostate carcinogenesis. Int J Cancer. **57**: 224–228. 1994. [Medline] [CrossRef]
14. Shirai T, Sano M, Imaida K, Takahashi S, Mori T, and Ito N. Duration dependent induction of invasive prostatic carcinomas with pharmacological dose of testosterone propionate in rats pretreated with 3,2'-dimethyl-4-aminobiphenyl and development of androgen-independent carcinomas after castration. Cancer Lett. **83**: 111–116. 1994. [Medline] [CrossRef]
15. Shirai T, Tamano S, Sano M, Imaida K, Hagiwara A, Futakuchi M, Takahashi S, and Hirose M. Site-specific effects of testosterone propionate on the prostate of rat pretreated with 3,2'-dimethyl-4-aminobiphenyl: dose-dependent induction of invasive carcinomas. Jpn J Cancer Res. **86**: 645–648. 1995. [Medline] [CrossRef]
16. Cui L, Mori T, Takahashi S, Imaida K, Akagi K, Yada H, Yaono M, and Shirai T. Slight promotion effects of intermittent administration of testosterone propionate and/or diethylstilbestrol on 3,2'-dimethyl-4-aminobiphenyl-initiated rat prostate carcinogenesis. Cancer Lett. **122**: 195–199. 1998. [Medline] [CrossRef]
17. Valastyan S, and Weinberg RA. Tumor metastasis: molecular insights and evolving paradigms. Cell. **147**: 275–292. 2011. [Medline] [CrossRef]
18. Barron DA, and Rowley DR. The reactive stroma microenvironment and prostate cancer progression. Endocr Relat Cancer. **19**: R187–R204. 2012. [Medline] [CrossRef]
19. Otranto M, Sarrazy V, Bonte F, Hinz B, Gabbiani G, and Desmouliere A. The role of the myofibroblast in tumor stroma remodeling. Cell Adh Migr. **6**: 203–219. 2012. [Medline] [CrossRef]
20. Orimo A, and Weinberg RA. Heterogeneity of stromal fibroblasts in tumors. Cancer Biol Ther. **6**: 618–619. 2007. [Medline] [CrossRef]
21. Webber MM, Trakul N, Thraves PS, Bello-DeOcampo D, Chu WW, Storto PD, Huard TK, Rhim JS, and Williams DE. A human prostatic stromal myofibroblast cell line WPMY-1: a model for stromal-epithelial interactions in prostatic neoplasia. Carcinogenesis. **20**: 1185–1192. 1999. [Medline] [CrossRef]
22. Desai KV, and Kondaiah P. Androgen ablation results in differential regulation of transforming growth factor-β isoforms in rat male accessory sex organs and epididymis. J Mol Endocrinol. **24**: 253–260. 2000. [Medline] [CrossRef]
23. Sampson N, Koziel R, Zenzmaier C, Bubendorf L, Plas E, Jansen-Durr P, and Berger P. ROS signaling by NOX4 drives fibroblast-to-myofibroblast differentiation in the diseased prostatic stroma. Mol Endocrinol. **25**: 503–515. 2011. [Medline] [CrossRef]
24. Kojima Y, Acar A, Eaton EN, Mellody KT, Scheel C, Ben-Porath I, Onder TT, Wang ZC, Richardson AL, Weinberg RA, and Orimo A. Autocrine TGF-β and stromal cell-derived factor-1 (SDF-10 signaling drives the evolution of tumor-promoting mammary stromal myofibroblasts. Proc Natl Acad Sci USA. **107**: 20009–20014. 2010. [Medline] [CrossRef]
25. Wang J, Ying G, Wang J, Jung Y, Lu J, Zhu J, Pienta KJ, and Taichman RS. Characterization of phosphoglycerate kinase-1 expression of stromal cells derived from tumor microenvironment in prostate cancer progression. Cancer Res. **70**: 471–480. 2010. [Medline] [CrossRef]

Oncogene (2014) **33,** 2273–2278

www.nature.com/onc

SHORT COMMUNICATION

ANGPTL4 is a secreted tumor suppressor that inhibits angiogenesis

E Okochi-Takada[1], N Hattori[1], T Tsukamoto[2], K Miyamoto[3], T Ando[1,4], S Ito[5], Y Yamamura[5], M Wakabayashi[1], Y Nobeyama[1,6] and T Ushijima[1]

Tumor suppressors with extracellular function are likely to have advantages as targets for cancer therapy, but few are known. Here, we focused on angiopoietin-like 4 (ANGPTL4), which is a secreted glycoprotein involved in lipoprotein metabolism and angiogenesis, is methylation-silenced in human cancers, but has unclear roles in cancer development and progression. We found a deletion mutation in its coiled-coil domain at its N-terminal in human gastric cancers, in addition to hypermethylation of the *ANGPTL4* promoter CpG islands. Forced expression of wild-type *ANGPTL4*, but not *ANGPTL4* with the deletion, at physiological levels markedly suppressed *in vivo* tumorigenicity and tumor angiogenesis, indicating that the latter caused the former. Tumor-derived ANGPTL4 suppressed *in vitro* vascular tube formation and proliferation of human umbilical vascular endothelial cells, partly due to suppression of ERK signaling. These showed that ANGPTL4 is a genetically and epigenetically inactivated secreted tumor suppressor that inhibits tumor angiogenesis.

Oncogene (2014) **33,** 2273–2278; doi:10.1038/onc.2013.174; published online 20 May 2013

Keywords: epigenetics; angiogenesis; tumor suppressor; gastric cancer; DNA methylation

INTRODUCTION

Tumor-suppressor genes (TSGs) are somatically inactivated by genetic and/or epigenetic mechanisms.[1,2] Targeting TSGs for molecular target therapy has been attempted mainly for *p53*.[3,4] However, the attempts have not been easy, partly due to the fact that the *p53* gene product is neither a cell surface protein nor a typical enzyme.[5] Considering efficient delivery to targets, TSGs whose products function extracellularly as secreted proteins are likely to have advantages. So far, secreted frizzled-related proteins are known as secreted tumor suppressors,[6,7] but few others are known.

As a candidate, we previously identified that angiopoietin-like 4 (*ANGPTL4*), a member of the angiopoietin-like family, was silenced by aberrant DNA methylation of promoter CpG islands (CGIs) (methylation-silenced) in human cancers.[8,9] ANGPTL4 is a secreted glycoprotein, and is involved in lipoprotein metabolism through inhibition of lipoprotein lipase.[10] In contrast, the role of ANGPTL4 in angiogenesis remains controversial.[11–15] Likewise, its role in tumor formation also remains controversial—some reports suggesting its tumor-suppressive function[12,16,17] and others its oncogenic function.[18–20]

Here, we aimed to clarify the role of ANGPTL4 in cancer development and progression and also in tumor angiogenesis.

RESULTS AND DISCUSSION

Inactivation of *ANGPTL4* by epigenetic and genetic mechanisms in human gastric cancers

ANGPTL4 methylation was detected in 10 of 91 human gastric cancers (11%) by quantitative real-time methylation-specific PCR (Figure 1a). The mRNA and protein expression levels of ANGPTL4 in cancers with *ANGPTL4* methylation were significantly lower than those in cancers without methylation (Supplementary Figure S2). Methylation status did not have any association with clinicopathological features, but had a significant association with Epstein-Barr virus infection status and the presence of the CGI methylator phenotype[21] (Supplementary Figure S1 and Supplementary Table S1). In non-cancerous gastric mucosae of 71 gastric cancer patients and gastric mucosae of 58 healthy volunteers, the methylation level was also quantified. It was significantly higher in cancer patients than in healthy volunteers and in individuals with *H. pylori* infection than in those without (Figure 1b). This suggested the potential involvement of *ANGPTL4* methylation in the formation of an epigenetic field for cancerization, a predisposed normal-appearing tissue.[22]

ANGPTL4 mutation was then analyzed in 89 of the 91 gastric cancers (due to sample availability), and a somatic 21-bp deletion in exon 1 was identified in one specimen (cancer #217T) without *ANGPTL4* methylation (Figures 1c and d). ANGPLT4 consists of an N-terminal coiled-coil domain (CCD) and a C-terminal fibrinogen-like domain,[23,24] and the 21-bp deletion was located in the CCD (Supplementary Figure S3). The CCD is reported to be critical for regulation of the anti-angiogenic activity of ANGPTL4,[13] and the deletion here involved one of the two cysteine residues (Cys76 and Cys80) essential for the activity regulation by oligomerization.[25,26]

Loss of heterozygosity (LOH), which suggests the presence of a TSG,[27] was detected in 4 of 16 samples (25%) informative for a C/T polymorphism at the second position of codon 266. The locus of

[1]Division of Epigenomics, National Cancer Center Research Institute, Tokyo, Japan; [2]Oncological Pathology Division, Aichi Cancer Center Research Institute, Nagoya, Japan; [3]Division of Molecular Oncology, National Hospital Organization Kure Medical Center and Chugoku Cancer Center, Kureshi, Japan; [4] Third Department of Internal Medicine, University of Toyama, Toyama, Japan; [5]Department of Gastroenterological Surgery, Aichi Cancer Center Central Hospital, Nagoya, Japan and [6]Department of Dermatology, The Jikei University School of Medicine, Tokyo, Japan. Correspondence: Dr T Ushijima, Division of Epigenomics, National Cancer Center Research Institute, 5-1-1 Tsukiji, Chuo-ku, Tokyo 104-0045, Japan.
E-mail: tushijim@ncc.go.jp
Received 27 September 2012; revised 14 February 2013; accepted 28 March 2013; published online 20 May 2013

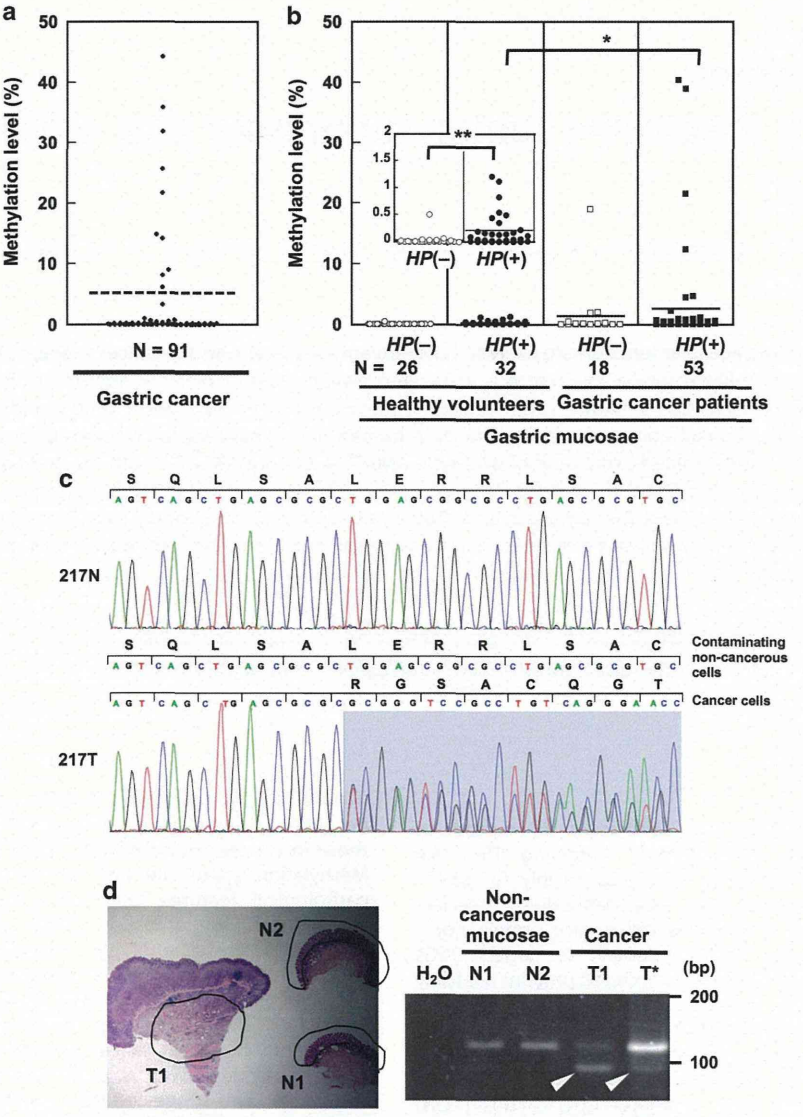

Figure 1. Aberrant methylation and a mutation of *ANGPTL4* in human gastric cancers, and methylation in non-cancerous gastric mucosae. (**a**) *ANGPTL4* methylation levels in gastric cancer specimens. Cancer samples were obtained from 91 gastric cancer patients undergoing gastrectomy with informed consents and approval by the institutional review boards. Some of the samples and methylation data were obtained from our previous study.[33] Quantitative real-time methylation-specific PCR was conducted with sodium bisulfite-treated DNA and primer sets specific to methylated and unmethylated sequences (Supplementary Table S2). Using a cutoff value of 6% (broken line), as in previous studies,[34–36] 10 cancer specimens were considered to have aberrant methylation. (**b**) *ANGPTL4* methylation levels in gastric mucosae of 58 healthy volunteers (30 male and 28 female; average age = 55 years) and 71 non-cancerous gastric mucosae of gastric cancer patients (50 male and 21 female; average age = 67 years) obtained by endoscopic biopsy of the antral region. *H. pylori* infection status was analyzed by a serum anti-*H. pylori* IgG antibody test (SRL, Tokyo, Japan), rapid urease test (Otsuka, Tokushima, Japan) or culture test (Eiken, Tokyo, Japan). The methylation level in gastric mucosae was significantly higher in gastric cancer patients than in healthy volunteers. The mean methylation level is shown by a horizontal line. $*P<0.05$, $**P<0.01$ (the unpaired Welch's *t*-test, two-sided). (**c**) A deletion mutation in a human gastric cancer specimen. All the seven exons and splice donor/acceptor sites of *ANGPTL4* were amplified by PCR (Supplementary Table S2), and the PCR products were directly cycle sequenced. The sequences of a gastric cancer specimen (217T) and its corresponding non-cancerous tissue (217N) between nucleotides 385 and 423 are shown. A 21-bp deletion in exon 1 was detected (shown in the gray background). (**d**) Confirmation of the deletion mutation using DNA samples obtained from a single tissue section. A 117-bp region encompassing the deletion was amplified by PCR, and the deletion was detected as a PCR product with a shorter size (96 bp). DNA from the cancer (T1), but not that from non-cancerous areas (N1 and N2), yielded the shorter product (shown by arrows). T*, genomic DNA extracted from frozen tumor tissues. If LOH was present in T1, the band intensity ratio was expected to be 1:1 (wild type:deletion mutant) (fraction of cancer cells was pathologically assessed to be 61–67%). If LOH was not present, it was expected to be 2:1. The ratio observed was ~1:2, and LOH was considered to be present in T1.

ANGPTL4, 19p13.3, has been suggested to contain TSGs, due to frequent LOH of the region in several types of cancers, such as pancreatic and colon cancers.[28–30] In addition, two human gastric cancer cell lines (MKN28 and AGS) without *ANGPTL4* expression had methylation of its promoter, and their treatment with 5-aza-2′-deoxycytidine (5-aza-dC), a DNA methylation inhibitor,

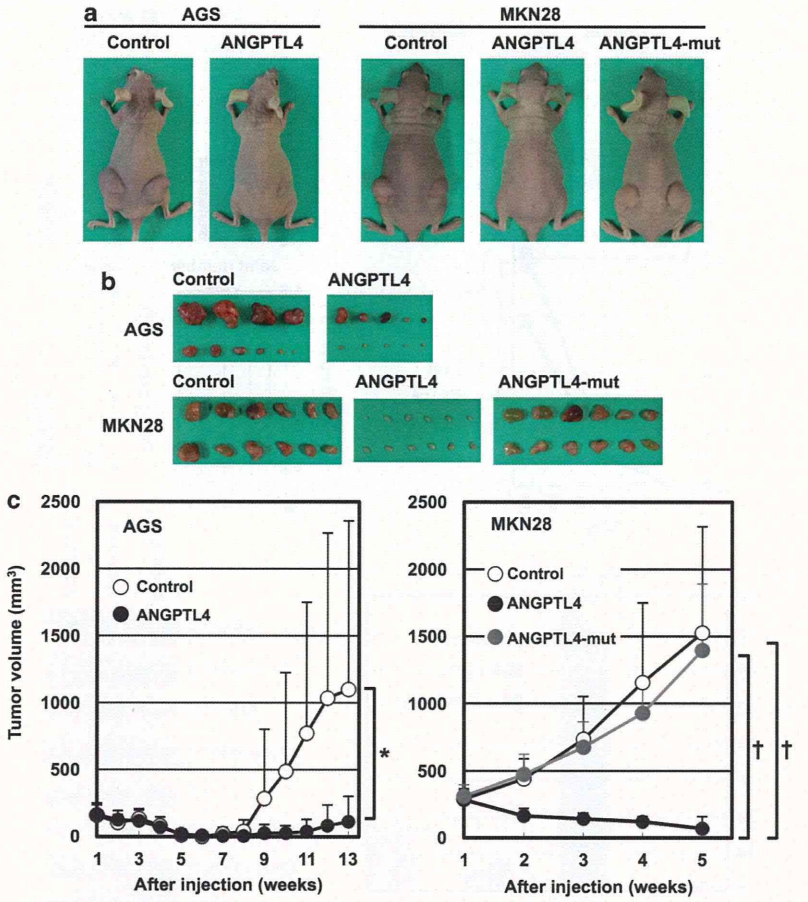

Figure 2. The effect of *ANGPTL4* and its mutant with the 21-bp deletion on tumor formation. The complementary DNA of wild-type *ANGPTL4*, its mutant with the deletion, and *EGFP* as a control were inserted into a mammalian expression vector pIRESpuro3 with the human cytomegalovirus immediate early promoter (Clontech, Mountain View, CA, USA). Individual vectors were transfected into MKN28 or AGS gastric cancer cell lines, and transfectants were selected with puromycin (0.3 μg/ml). Athymic nude mice (BALB/cAJc1-nu/nu, CLEA, Tokyo, Japan) were subcutaneously injected with cells (1×10^7 cells) mixed with an equal volume of Matrigel (BD Biosciences, San Diego, CA, USA). All the animal experiments were approved by the Committee for Ethics in Animal Experimentation, and conducted in accordance with the Guidelines for Animal Experiments of the National Cancer Center. (**a**) Representative photographs of transplanted tumors at 13 weeks (AGS) and 5 weeks (MKN28). *ANGPTL4* markedly suppressed tumor formation, while its mutant with the deletion lacked the activity. (**b**) Macroscopic views of the tumors resected at 13 weeks (AGS) and at 5 weeks (MKN28). Introduction of *ANGPTL4* markedly suppressed tumor sizes in both cell lines. The variable degree of suppression in AGS might have been due to the lower ANGPTL4 expression level (Supplementary Figure S5c). (**c**) Tumor growth curves after the injection. The volume of tumor (mm^3) was calculated by the formula: (length × $width^2$)/2. A tumor volume is shown as a mean ± s.d. ($N = 10$ in AGS and $N = 12$ in MKN28). $^*P < 0.05$, $^\dagger P < 0.001$ (Student's *t*-test).

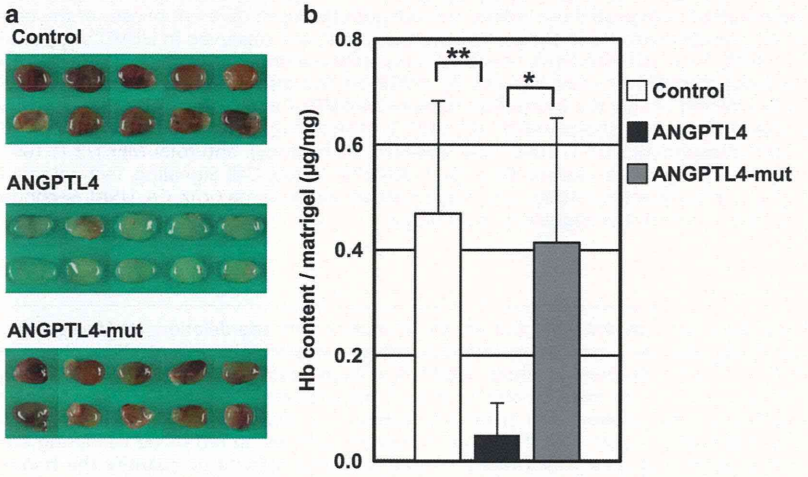

Figure 3. For caption please see page 2276.